Maternal Circulating MicroRNAs Control the Placental Response to Alcohol

[1]Alexander M. Tseng, [1]Amanda H. Mahnke, [2,3]Alan B. Wells, [1]Nihal A. Salem, [4]Andrea M. Allan, [5]Victoria H.J. Roberts, [6]Natali Newman, [6]Nicole A.R. Walter, [6]Christopher D. Kroenke, [6]Kathleen A. Grant, [7]Lisa K. Akison, [7]Karen M. Moritz, [2,3†]Christina D. Chambers, [1†]Rajesh C. Miranda & [#]CIFASD

[1]Department of Neuroscience and Experimental Therapeutics, Texas A&M University Health Science Center, Bryan, TX, USA

[2]Clinical and Translational Research Institute, University of California San Diego, San Diego, CA, USA

[3]Department of Pediatrics, University of California San Diego, San Diego, CA, USA

[4]Department of Neurosciences, University of New Mexico, Albuquerque, NM, USA

[5]Division of Reproductive and Developmental Sciences, Oregon National Primate Research Center, Oregon Health & Science University, Portland, OR, USA

[6]Division of Neuroscience, Oregon National Primate Research Center, Oregon Health & Science University, Portland, OR, USA

[7]Child Health Research Centre and School of Biomedical Sciences, the University of Queensland, 4072, Brisbane, Australia

[†] Co-senior authors to whom correspondence should be addressed:

Dr. Rajesh Miranda,

23 email: miranda@medicine.tamhsc.edu

24 Texas A&M University Health Science Center, College of Medicine, Department of Neuroscience

25 & Experimental Therapeutics, Medical Research and Education Building 8447 Riverside

26 Parkway, Bryan, TX 77807-3260

27 Phone: 979-436-0332 Fax: 979-436-0086

28 Dr. Christina Chambers

29 email: chchambers@ucsd.edu

30 University of California San Diego, Department of Pediatrics, 9500 Gilman Drive MC 0828, La

31 Jolla, CA 92093

32 Phone: 858-246-1704, Fax: 858246-1701

33 [#]CIFASD, Collaborative Initiative on Fetal Alcohol Spectrum Disorders

34

35 Acknowledgements:

36 This research was supported by grants from the NIH, P50 AA022534 (AMA), U01 AA014835 and

37 the Office of Dietary Supplements (CDC), R24 AA019431 (KAG), R01 AA021981 (CDK), R01

38 AA024659 (RCM), F31 AA026505 (AMT) and support from National Health and Medical

39 Research Council of Australia (KMM). We thank CIFASD for intellectual support and Megan S.

40 Pope and Tenley E. Lehman for their assistance in conducting cell culture and animal studies.

41 Data on human subjects is deposited at CIFASD.org, in accordance with NIH data repository

42 guidelines.

43

44 **Conflict of Interest Statement**

The authors have declared that no conflict of interest exists.

Abstract

We previously identified 11 miRNAs which were significantly elevated in the plasma of mothers whose infants were affected by maternal alcohol consumption (Heavily Exposed Affected: HEa) compared to infants who were apparently unaffected by alcohol exposure (Heavily Exposed Unaffected: HEua) or unexposed (UE) controls. These $_{HEa}$miRNAs were predicted to influence epithelial-mesenchymal transition (EMT), a pathway which is essential for fetal and placental growth and maturation. We now report that prenatal alcohol exposure (PAE) inhibits expression of placental EMT pathway members in rodent and non-human primate voluntary alcohol consumption models. Furthermore, in non-human primates, $_{HEa}$miRNAs mediated effects of PAE on EMT pathway inhibition. To directly investigate the interaction between $_{HEa}$miRNAs and ethanol on placenta, we assessed their effects on the cytotrophoblastic BeWO and extravillous/invasive HTR8 human trophoblast cell lines. When administered together, but not separately, $_{HEa}$miRNAs retarded the cell cycle, significantly impaired expression of core EMT pathway members, and reduced the invasiveness of trophoblasts, pointing to their collective role in modulating the placental growth and invasion deficits seen in PAE. $_{HEa}$miRNAs additionally interfered with maturation-dependent calcium dynamics, while promoting syncytialization-dependent increases in placental hormone expression. Finally, a single systemic administration of $_{HEa}$miRNAs, together, to pregnant mice, resulted in decreased fetal and placental growth. Taken together, our data suggests that, following PAE, $_{HEa}$miRNAs interfere with placental development and disrupt the EMT pathway, thereby contributing to the pathology of Fetal Alcohol Spectrum Disorders.

67 **Introduction**

68 Alcohol use during pregnancy remains prevalent despite published prevention
69 guidelines (1). Globally, a recent meta-analysis determined the prevalence of alcohol use during
70 pregnancy at 9.8% (2). Within the United States, a 2013 study found 18% of women reported
71 alcohol consumption during pregnancy, and 6.6% engaged in binge-drinking episodes, which
72 are particularly damaging to fetal development (3). In the state of Texas, we recently reported
73 an average state-wide third-trimester rate of alcohol exposure of 8.4%, with rates as high as
74 17.7% in some localities, suggesting high-rates of longitudinal alcohol consumption throughout
75 pregnancy (4).

76 Prenatal alcohol exposure (PAE) harms the developing embryo and fetus and results in a
77 constellation of negative infant outcomes, including craniofacial dysmorphologies, growth
78 retardation, and neurobehavioral abnormalities, collectively termed Fetal Alcohol Spectrum
79 Disorders (FASDs) (5). Estimates for the prevalence of FASDs range from 2-5% of the school age
80 population in the US and Western Europe (6) to 13.6-20.9% in South Africa (7). Estimates for
81 the global prevalence of fetal alcohol syndrome (FAS), the most severe end of the FASD
82 continuum, characterized by cranio-facial dysmorphologies, growth restriction, and CNS
83 abnormalities, range from 0.15 to 0.3% (8, 9), but are much higher in specific populations, for
84 example, as high as 5.9-9.1% in the Cape Coloured (mixed ancestry) community in South Africa
85 (7).

86 Given the lifelong debility and economic burden associated with FASDs (10), there is an
87 urgent need to develop sensitive and specific methodologies to identify affected children early
88 in development, as well as develop interventions which can mitigate the effects of PAE on the

89 developing fetus. In 2016, we reported that elevated levels of 11 distinct microRNAs (miRNAs)
90 in 2nd and 3rd trimester maternal circulation distinguished infants who were affected by in-utero
91 alcohol exposure (Heavily Exposed Affected: HEa) from those who were apparently unaffected
92 at birth by PAE (Heavily Exposed Unaffected: HEua), or those who were unexposed (UE) (11) .
93 We predicted that these $_{HEa}$miRNAs (MIMAT0004569 [hsa-miR-222-5p], MIMAT0004561 [hsa-
94 miR-187-5p], MIMAT0000687 [hsa-mir-299-3p], MIMAT0004765 [hsa-miR-491-3p],
95 MIMAT0004948 [hsa-miR-885-3p], MIMAT0002842 [hsa-miR-518f-3p], MIMAT0004957 [hsa-
96 miR-760], MIMAT0003880 [hsa-miR-671-5p], MIMAT0001541 [hsa-miR-449a], MIMAT0000265
97 [hsa-miR-204-5p], MIMAT0002869 [has-miR-519a-3p]) in addition to being biomarkers of infant
98 outcome following PAE, influence signaling pathways crucial for early development, particularly
99 the epithelial-mesenchymal transition (EMT) pathway.
100 Placental development involves maturation of the cytotrophoblasts at the tip of
101 anchoring villi into invasive extravillous trophoblasts, as well as fusion of cytotrophoblasts into
102 multinucleate, hormone-producing syncytiotrophoblasts (12). Maturation into extravillous
103 trophoblasts, which invade the maternal decidua and remodel the uterine spiral arteries into
104 low-resistance high-flow vessels that enable optimal perfusion for nutrient and waste
105 exchange, requires cytotrophoblasts to undergo EMT (13). Impaired placental EMT, as well as
106 orchestration of the opposing mesenchymal-epithelial transition pathway, has been found in
107 conditions resulting from placental malfunction, primarily preeclampsia (14-19). While there
108 have been no previous studies directly investigating the effects of PAE on placental EMT, a
109 rodent study demonstrated that PAE, during a broad developmental window, reduced the
110 number of invasive trophoblasts within the mesometrial triangle, a region of the uterine horn

111 directly underlying the decidua (20). Furthermore, both human and rodent studies have found
112 PAE disrupts placental morphology, and interferes with cytotrophoblast maturation, as with
113 preeclampsia (21-24). Our study is the first to report on PAE induced impairment of the
114 placental EMT pathway in both rodents and primates. We are also the first to report that PAE
115 elevates human chorionic gonadotropin (hCG) levels in the third trimester, a finding mirrored in
116 other developmental pathologies including preeclampsia, intrauterine growth restriction, and
117 Down's syndrome (25-28). Ultimately, we propose that $_{HEa}$miRNAs may mediate impairment in
118 the EMT pathway and elevated hCG levels due to PAE.
119

120 **Methods**

121 Animal models:

122 All rodent experiments were performed in accordance with protocols approved by the
123 University of New Mexico Institutional Animal Care and Use Committee (IACUC), the Texas
124 A&M University IACUC, as well as the University of Queensland Anatomical Bioscience Animal
125 Ethics Committee. All procedures involving non-human primate research subjects were
126 approved by the IACUC of the Oregon National Primate Research Center (ONPRC), and
127 guidelines for humane animal care were followed. The ONPRC abides by the Animal Welfare Act
128 and Regulations enforced by the US Department of Agriculture.

129 Mouse model of PAE:

130 C57/BL6J mice (Jackson Laboratory, Bar Habor, ME) were housed under reverse 12-hour dark /
131 12-hour light cycle (lights off at 08:00 hours). PAE was performed using a previously described
132 limited access paradigm of maternal drinking (29, 30). Briefly, 60-day old female mice were
133 subjected to a ramp-up period with 0.066% saccharin containing 0% ethanol (2 days), 5%
134 ethanol (2 days), and finally 10% ethanol for 4-hours daily from 10:00–14:00 beginning 2 weeks
135 prior to pregnancy, continuing through gestation (Supplementary Figure 2A). Female mice
136 offered 0.066% saccharin without ethanol during the same time-period throughout pregnancy
137 served as controls. Tissue from the labyrinth, junctional, and decidual zone of male and female
138 gestational day 14 (GD14) placentae were microdissected, snap-frozen in liquid nitrogen, and
139 stored at -80ºC preceding RNA and protein isolation.

140 Mouse model for $_{HEa}$miRNA overexpression:

141 For systemic administration of miRNAs, previously nulliparous C57/BL6NHsd dams (Envigo,
142 Houston, TX) were tail-vein-injected on GD10 with either 50 µg of miRNA miRVana™ mimic
143 negative control (Thermo Fisher, Waltham, MA, Cat No. 4464061) or pooled $_{HEa}$miRNA
144 miRVana™ mimics in In-vivo RNA-LANCEr II (Bioo Scientific, Austin, TX, 3410-01), according to
145 manufacturer instructions. The 50 µg of pooled $_{HEa}$miRNA mimics consisted of equimolar
146 quantities of mmu-miR-222-5p, mmu-miR-187-5p, mmu-mir-299a, mmu-miR-491-3p, miR-760-
147 3p, mmu-miR-671-3p, mmu-miR-449a-5p, and mmu-miR-204-5p mimics. GD10 is a time point
148 near the beginning of the developmental period of branching morphogenesis, immediately
149 following chorioallantoic attachment, during which the placenta invades the maternal
150 endometrium (31). At GD18, pregnancies were terminated with subsequent quantification of
151 fetal weight, crown-rump length, snout-occipital distance, biparietal diameter, placental
152 weight, width, and thickness (Figure 13A).
153 Rat model of PAE:
154 Outbred nulliparous Sprague-Dawley rats were housed under a 12-hour light/12-hourdark
155 cycle. PAE in Sprague-Dawley was conducted according to our previously published exposure
156 paradigm (23, 32). Briefly, dams were given a liquid diet containing either 0% or 12.5% ethanol
157 (vol/vol) from 4 days prior to mating until GD4 (Supplementary Figure 2B). Dams had *ad libitum*
158 access to the liquid diet 21-hours daily and consumed equivalent calories. Water offered during
159 the remaining 3-hours of the day. On GD5, liquid diets were removed and replaced with
160 standard laboratory chow. On GD20, placentas were immediately separated into the labyrinth
161 and junctional zone, snap frozen in liquid nitrogen and stored at −80 °C preceding RNA
162 isolation.

163 Non-human primate model of PAE:

164 As previously described in detail (33), adult female rhesus macaques were trained to orally self-
165 administer either 1.5 g/kg/d of 4% ethanol solution (equivalent to 6 drinks/day), or an isocaloric
166 control fluid prior to time-mated breeding. Each pregnant animal continued ethanol exposure
167 until gestational day 60 (GD60, term gestation is 168 days in the rhesus macaque) (34).
168 Pregnancies were terminated by cesarean section delivery at three different time points; GD85,
169 GD110, or GD135 (Supplementary Figure 2C). The macaque placenta is typically bi-lobed with
170 the umbilical cord insertion in the primary lobe and bridging vessels supplying the fetal side
171 vasculature to the secondary lobe (Figure 2E showing gross placenta anatomy) (35) . Full
172 thickness tissue biopsies (maternal decidua to fetal membranes) were taken from both the
173 primary and secondary lobes of the placenta (Figure 2E showing H&E section of placenta).
174 Samples were immediately snap-frozen in liquid nitrogen and stored at -80°C preceding RNA
175 isolation.

176 Cell culture trophoblast models:

177 BeWO human cytotrophoblastic choriocarcinoma cells and HTR-8/SVneo extravillous cells were
178 sourced from ATCC (Manassas, VA, Cat No. CCL-98 and CRL-3271 respectively). BeWO cells
179 were maintained in HAM's F12 media containing penicillin (100 U/ml), streptomycin (100
180 µg/ml), and 10% vol/vol fetal calf serum (FCS) at 37°C and 5% CO_2. HTR8 cells were maintained
181 in RPMI-1640 media with 5% vol/vol FCS, under otherwise identical conditions. Culture medium
182 was replenished every 2 days and cells sub-cultured every 4-5 days.
183 BeWO cells were treated with 20 µm forskolin to induce syncytialization, as previously
184 described (36, 37). BeWO and HTR8 cells were also subjected to four separate ethanol

185 treatment conditions: 0 mg/dL, 60 mg/dl (13 mM),120 mg/dl (26 mM) or 320 mg/dl (70 mM).

186 To achieve HEamiRNA overexpression and inhibition, Dharmacon miRIDIAN™ miRNA mimics and

187 hairpin inhibitors [25 nM] were transfected into subconfluent BeWO and HTR8 cells using

188 RNAIMAX lipofection reagent (Thermo Fisher, Cat No. 13778).

189 Cell cycle analysis:

190 At 48-hours-post transfection, BeWO cells were pulsed with 10 µM EdU for 1-hour. Cells were

191 immediately harvested and cell cycle analysis was performed with the Click-iT® EdU Alexa

192 Fluor® 488 Flow Cytometry Assay Kit (Thermo Fisher, Cat No. C10420), in conjunction with 7-

193 Amino-Actinomycin D (Thermo Fisher, Cat No. 00-6993-50), according to manufacturer

194 instructions, using the Beckman Coulter® Gallios 2/5/3 Flow Cytometer. Data was analyzed

195 using Kaluza software (Beckman Coulter, Brea, CA).

196 Cell death analysis:

197 BeWO cell culture was harvested 48-hours post transfection media was subjected to lactate

198 dehydrogenase (LDH) detection using the Pierce™ LDH Cytotoxicity Assay Kit (Thermo Fisher,

199 Cat No. 88953), according to manufacturer instructions, for lytic cell death quantification. The

200 Promega Caspase-Glo® 3/7 Assay Systems (Promega, Madison, WI, Cat No. G8091) was used to

201 quantify apoptotic cell death

202 Invasion assay:

203 At 24-hours post-transfection and/or ethanol exposure, HTR8 cells were serum starved for an

204 additional 18-hours. Subsequently, HTR8 cells were seeded onto trans-well permeable supports

205 precoated with 300 µg/mL Matrigel (Corning, Corning, NY, Cat No. 354248). After 24-hours,

206 cells remaining in the apical chamber were removed with a cotton swab. Cells that invaded into

207 the basal chamber were incubated with 1.2 mM 3-(4,5-dimethylthiazol-2-yl)-2,5-
208 diphenyltetrazolium bromide (MTT) for 3-hours, and the precipitate solubilized with 10% SDS in
209 0.01N HCl. Absorbance intensities were read at 570 nm in a Tecan Infinite® 200 plate reader.
210 Metabolic flux analysis and calcium imaging:
211 BeWO cells (10,000/well) were plated into Seahorse XF96 Cell Culture Microplates (Agilent
212 Biotechnology, Cat No. 103275-100). The oxygen consumption rate (OCR), a measure of
213 mitochondrial respiration, and extracellular acidification rate (ECAR), a measure of glycolysis,
214 were measured using the Seahorse XFe96 flux analyzer (Seahorse Bioscience, North Billerica,
215 MA). At the time of assay, cell culture medium was replaced with the appropriate pre-warmed
216 Seahorse XF Base Medium (Agilent Biotechnology, Santa Clara, CA, Cat No. 102353-100). OCR
217 and ECAR parameters were measured using the Seahorse XFp Cell Energy Phenotype Test Kit™
218 (Agilent Biotechnology, Cat No. 103275-100).
219 BeWO cells were also plated onto glass coverslips in 24 well plates at a density of 30,000
220 cells/well. After exposure to ethanol and/or forskolin in culture, cells were prepared for calcium
221 imaging. After replacement of culture media with external imaging media (154 mM NaCl, 5 mM
222 KCl, 2 mM $CaCl_2$, 0.5 mM $MgCl_2$, 5 mM glucose, 10 mM HEPES, pH 7.4), cells were loaded for 35
223 minutes at 37°C with the calcium indicator dye fluo-4 AM (Thermo Fisher Scientific, Cat No.
224 F14201), at a final concentration of 5µM fluo-4 AM in 0.1% DMSO. After incubation, cells were
225 washed to remove remaining extracellular fluo-4 and imaged at 40x using confocal microscopy
226 (FV1200-equipped BX61WI microscope, Olympus Corporation, Center Valley, PA). Time-lapse
227 images were acquired at a frequency of 0.5Hz. Individual cells were manually outlined and area
228 and mean fluorescence intensity were obtained for each cell (FIJI image processing

229 package)(38) . To determine the functional calcium range of each cell, at the end of imaging,
230 cells were exposed to 5 µM ionomycin and 10 mM EGTA (0mM external Ca^{2+}, $F_{range} = F_{ionomycin}$-
231 F_{EGTA}). Baseline fluorescence was determined by averaging the lowest 5 consecutive
232 fluorescence values during the initial 5 minutes ($F_{baseline}$) which was then expressed as a
233 percentage of F_{range} ($\Delta F_{baseline} = (F_{baseline}-F_{EGTA})/F_{range}$ X100). Maximal intracellular calcium
234 response to 100 µM ATP was determined by averaging the highest 3 consecutive fluorescence
235 values during ATP application (F_{ATP}) and determining the amount of fluorescence as a
236 percentage of F_{range} ($\Delta F_{ATP} = (F_{ATP}-F_{EGTA})/F_{range}$ X100).
237 Quantitative reverse transcriptase-polymerase chain reaction (qRT-PCR) analysis:
238 Total RNA was extracted from tissue, well as BeWO and HTR8 cells, using the miRNeasy Mini kit
239 (Qiagen, Cat No. 217004). For miRNA qPCR assays, cDNA was synthesized from 200 ng of total
240 RNA using the miRCURY LNA Universal RT cDNA synthesis kit (Exiqon, Cat No. 203301/Qiagen,
241 Cat No. 339340, Germantown, MD) and expression was assessed using miRCURY LNA SYBR
242 Green (Exiqon, Cat No. 203401/Qiagen, Cat No. 339345). For mRNA qPCR assays, cDNA was
243 synthesized from 500 ng of total RNA using the qScript™ cDNA Synthesis Kit (Quanta/Qiagen,
244 Cat No. 95047). Gene expression analysis was performed using PerfeCTa SYBR Green FastMix
245 (Quanta, Cat No. 95073) on the ViiA 7 Real-Time PCR System (Thermo Fisher Scientific). The
246 data presented correspond to the mean $2^{-\Delta\Delta Ct}$ after being normalized to β-actin. For each
247 primer pair, thermal stability curves were assessed for evidence of a single amplicon and the
248 length of each amplicon was verified using agarose gel electrophoresis. A list of primers and
249 their sequences is presented in Supplementary Table 1.
250 Western immunoblotting analysis:

251 Protein was extracted using 1X RIPA lysis buffer (Millipore Sigma, Burlington MA) supplemented
252 with Halt protease inhibitor cocktail (Thermo Fisher Scientific). Tissue was homogenized using
253 the Branson Sonifier 150. Protein concentration was determined using Pierce BCA protein assay
254 kit (Thermo Fisher Scientific) and 30 µg of protein was loaded onto a 4-12% Bis-Tris
255 (Invitrogen/Thermo Fisher Scientific, Cat No. NPO323BOX), size fractionated at 200 V for 35
256 minutes, and transferred to a PVDF membrane using the iBlot transfer system
257 (Invitrogen/Thermo Fisher Scientific). Blots with protein from cultured cells were blocked with
258 5% nonfat dry milk in tris-buffered saline containing Tween®-20 (TTBS) for 1-hour and
259 incubated overnight with primary antibody. The blot was then washed and incubated with an
260 HRP-conjugated goat anti-rabbit or anti-mouse IgG (Invitrogen) at dilution 1:1000 for 1-hour,
261 then developed using PerkinElmer Western Lightning Plus Chemi ECL (PerkinElmer; Waltham,
262 MA) and visualized using a CCD camera (Fluorchem Q, Alpha Innotech; San Leandro, CA). Blots
263 with protein from homogenized tissue were dried overnight, rehydrated in methanol, stained
264 with REVERT™ Total Protein Stain and developed with the Odyssey CLx Imaging System (LI-COR,
265 Lincoln, NE). Blots were then blocked with Odyssey® Blocking Buffer (TBS) for 1h and incubated
266 overnight with primary antibody. The blot was then washed and incubated with IRDye® 800CW
267 secondary antibody (LI-COR, Cat No. 925-32210). The following antibodies were used: β-Actin
268 HRP (Santa Cruz Biotechnology, Cat No. sc-47778); Goat anti-Mouse IgG (H+L) Secondary
269 Antibody, HRP (Thermo Fisher, Cat No. 62-6520); Goat anti-Rabbit IgG (H+L) Secondary
270 Antibody, HRP (Thermo Fisher, Cat No. 65-6120); purified Mouse Anti-E-Cadherin (BD
271 Biosciences, Cat No. 610181), Rabbit anti-vimentin antibody [EPR3776] (Abcam, Cat No. ab

272 924647). Protein levels were quantified using the densitometric analysis package in FIJI image
273 processing software (38).

274 ELISA:

275 The 2nd and 3rd trimester maternal plasma samples were collected as part of a longitudinal
276 cohort study conducted in two regions of Western Ukraine as part of the Collaborative Initiative
277 on Fetal Alcohol Spectrum Disorders (CIFASD.org) between the years 2006 and 2011, as
278 previously reported(11). Plasma, at a 1:1000 dilution, was subjected to hCG detection using
279 Abcam's intact human hCG ELISA kit (Cat no. ab100533) following the manufacturer's protocol.

280 Literature Review

281 We conducted a literature review for HEamiRNAs and their associated gestational pathology
282 using the National Institute of Health's Pubmed search interface. For each miRNA, the following
283 search parameters were used:

284 *[miRX OR miR X OR miRNA X OR miRNAX or miRNX] AND MeSH Term*

285 where X represents the miRNA of interest and automatic term expansion was enabled. The
286 following MeSH terms, and related search terms (in brackets), were used: Fetal Growth
287 Retardation [Intrauterine Growth Retardation, IUGR Intrauterine Growth Restriction, Low Birth
288 Weight, LBW, Small For Gestational Age, SGA], Premature Birth [Preterm Birth, Preterm Birth,
289 Preterm Infant, Premature Infant, Preterm Labor, Premature Labor], Spontaneous Abortion
290 [Early Pregnancy Loss, Miscarriage, Abortion, Tubal Abortion, Aborted Fetus], Pre-Eclampsia
291 [Pre Eclampsia, Preeclampsia, Pregnancy Toxemia, Gestational Hypertension, Maternal
292 Hypertension], and Maternal Exposure [Environmental Exposure, Prenatal Exposure]. Returned
293 articles were subsequently assessed for relevance.

294 Secondary analysis of RNA sequencing data:

295 Expression levels of $_{HEa}$miRNAs in tissues were determined using the Human miRNA Expression
296 Database and the miRmine Human miRNA expression database(39, 40). For expression analysis
297 of $_{HEa}$miRNA pri-miRNAs, RNA sequencing data was used from NCBI's sequence read archive
298 (https://www.ncbi.nlm.nih.gov/sra). The accession numbers for the sequence files are: uterus
299 (SRR1957209), thyroid (SRR1957207), thymus (SRR1957206), stomach (SRR1957205), spleen
300 (SRR1957203), small intestine (SRR1957202), skeletal muscle (SRR1957201), salivary gland
301 (SRR1957200), placenta (SRR1957197), lung (SRR1957195), liver (SRR1957193), kidney
302 (SRR1957192), heart (SRR1957191), whole brain (SRR1957183), adrenal gland (SRR1957124),
303 bone marrow (ERR315396), colon (ERR315484), adipose tissue (ERR315332), and pancreas
304 (ERR315479). Deep sequencing analysis was conducted using the Galaxy version 15.07 user
305 interface according to the bioinformatics pipeline outlined in Supplementary Figure 1.

306 Statistical analyses:

307 Linear regression models were used to estimate associations between infant growth measures
308 and miRNA expression levels, gestational age at blood draw, the interaction between subject-
309 centered miRNA expression level and gestational age at blood draw, and child sex. Spearman
310 correlations between infant growth measures and subject-centered miRNA expression levels
311 were also calculated.

312 Linear regression models were also used to estimate the associations between gestational at
313 birth and log-transformed hCG levels, ethanol intake, the interaction between log-transformed
314 hCG levels and ethanol intake, gestational at blood draw, and child sex.

315 Statistical Analysis and graphs were generated with GraphPad Prism 6 software (GraphPad
316 Software, Inc., La Jolla, CA), SPSS v24, or R version 3.3.1. Results are expressed as the mean ±
317 SEM. The overall group effect was analyzed for significance using 1-way MANOVA, 1-way or 2-
318 way ANOVA with Tukey's HSD or Sidak's post-hoc testing when appropriate. A 2-tailed
319 Student's t-test was used for planned comparisons. All statistical tests, sample-sizes, and post-
320 hoc analysis are appropriately reported in the results section. Results are expressed as the
321 mean ± SEM. A value of $p < 0.05$ was considered statistically significant, an a value of $0.1 < p <$
322 0.05 was considered marginally significant

323 Author contributions:

324 AT, RM and CC conceived of and planned the study. AT, AM, and NS designed and conducted
325 cell culture studies, and AT conducted in vivo, murine miRNA overexpression studies and
326 analyzed tissues from mouse, rat and primate PAE models. AA developed the mouse PAE model
327 and LA and KM developed the rat PAE model and provided tissues. VR, NN, CK and KG
328 developed the non-human primate model of PAE and provided RNA from microdissected
329 tissues. AW and CC performed statistical analyses of human studies. AT, AM and RCM
330 collaborated on all other statistical analyses. AT, AM, AW, NS, AA, VR, NN, CK, KG, CC, and RM
331 collaborated in preparing the manuscript.

332

333

334

335 **Results**

336 HEamiRNAs are implicated in placental-associated pathologies

337 Outside of our report that elevated HEamiRNA levels predict infant outcomes following
338 PAE, few other studies have investigated expression of these miRNAs in the context of PAE or
339 other potentially toxic prenatal exposures (Figure 1A) (41-48). Subsequently, given our
340 prediction that HEamiRNAs interfere with signaling pathways governing fetal and placental
341 development, we conducted a literature review of reports on HEamiRNA levels in gestational
342 pathologies which, as with PAE, include aberrant placentation as an etiological factor (49-51).
343 Surprisingly, placental and plasma levels of 8 out of 11 of these HEamiRNAs were significantly
344 dysregulated in one or more of these gestational pathologies with expression of the majority of
345 these 8 miRNAs altered in both fetal growth restriction and preeclampsia (Figure 1B) (45, 46,
346 48, 52-69), both of which are characterized by poor placental invasion as an etiological factor
347 (70-76).

348 HEamiRNAs explain variance in infant growth outcomes due to PAE

349 Given the association of individual HEamiRNAs with gestational pathologies, we sought to
350 determine if circulating HEamiRNAs levels could explain the variance in sex and gestational age-
351 adjusted neonatal height, weight and head circumference in our Ukrainian birth cohort, which
352 are growth measures sensitive to in utero environment (77). We found that 8 of the HEamiRNAs
353 significantly explained between 7 to 19% of infant variation in these growth measures
354 (Supplementary Table 2). Furthermore, 7 of these miRNAs were also associated with fetal
355 growth restriction and preeclampsia as identified by our literature review. Additionally, only 1

356 of the 3 miRNAs not previously-reported to be associated with gestational pathologies was
357 correlated with measures of fetal growth and development in our dataset (Figure 1B).

358 $_{HEa}$miRNAs are transcribed preferentially in the placenta

359 Interestingly, data extracted from publicly available gene expression profiling datasets
360 show that $_{HEa}$miRNAs as well as $_{HEa}$pri-miRNAs are enriched in placenta compared to other
361 tissues, suggesting that the placenta transcribes these miRNAs and may be a significant
362 contributory tissue to maternal circulating $_{HEa}$miRNAs (Figures 1C and D) (40). Since chorionic
363 villi are immersed in maternal blood, it is possible that the placenta is both the source and a
364 target of maternal $_{HEa}$miRNAs. Moreover, since $_{HEa}$miRNAs are also associated with a number of
365 gestational pathologies caused by poor placental invasion, these may also constitute a local
366 paracrine signal to coordinate the response of placental tissues to PAE. We therefore assessed
367 in rodent and primate models, whether PAE could result in impaired EMT, and if $_{HEa}$miRNAs
368 could explain the effects of PAE on placental EMT-associated gene expression.

369 $_{HEa}$miRNAs moderate placental EMT impairment in PAE models

370 In the first analysis, using a murine model of PAE that mimicked moderate to binge-type
371 alcohol consumption throughout early and mid-pregnancy, we fractionated GD14 placenta into
372 three zones: the cytotrophoblast and syncytiotrophoblast rich labyrinth zone, the glycogen and
373 spongiotrophoblast rich junctional zone, and the decidual zone comprising the endometrial
374 contribution to the placenta (Figure 2A). Multivariate analysis of variance (MANOVA) for
375 expression of five core genes in the EMT pathway within placental trophoblasts (13, 78, 79)
376 revealed a significant effect of ethanol exposure on the EMT pathway selectively within the
377 labyrinth zone (Pillai's trace statistic, $F_{(5,21)}=6.85$, $p<0.001$, Figure 2B) but not within the

378 junctional or decidual zones. Post-hoc univariate ANOVA indicated ethanol exposure specifically
379 elevated *CDH1* ($F_{(1,25)}$=7.452, p=0.011), which encodes epithelial E-Cadherin, whereas
380 expression of the pro-mesenchymal transcription factor *SNAI1* was significantly reduced (Snail1,
381 $F_{(1,25)}$=21.022, p=0.0001). We also observed a trend towards decreased expression of the
382 terminal mesenchymal marker *VIM* (Vimentin, $F_{(1,25)}$=2.749, p=0.11), while there was no effect
383 on *TWIST* expression (Figures 3A-3E). Consistent with our gene expression data, E-Cadherin
384 protein levels were significantly elevated in the labyrinth zone of PAE placenta ($F_{(1,24)}$=31.63,
385 p=0.0005), while not in the junctional or decidual zones (Figure 3F and Supplementary Figures
386 3A and B). However, when we controlled for expression of the 8 mouse homologues of
387 $_{HEa}$miRNAs as a covariate, using multivariate analysis of covariance (MANCOVA), ethanol's effect
388 on EMT became marginally insignificant (Pillai's trace, $F_{(5,21)}$=2.713, p=0.068) (Figure 2C),
389 suggesting that these miRNAs partially mediate effects of PAE on the EMT pathway in mice.
390 Using a periconceptional model of ethanol exposure, we next assessed the effects of
391 PAE on EMT in rat placentas. As in mice, MANOVA revealed a significant effect of PAE on core
392 EMT gene expression within the labyrinth zone (Pillai's trace statistic, $F_{(5,24)}$=2.63, p=0.049,
393 Figure 2D). Post-hoc analysis indicates that PAE significantly elevated *CDH1* ($F_{(1,28)}$=4.366,
394 p=0.046) and *SNAI1* ($F_{(1,25)}$=4.949, p=0.034) whereas *VIM*, *SNAI2* (Snail2), and *TWIST* expression
395 were not significantly different from controls (Supplementary Figures 4A-E). However, unlike
396 our results in mice, a MANCOVA with the 8 rat homologues of $_{HEa}$miRNAs as a covariates did not
397 account for the effects of PAE on EMT, since the effect of PAE continued to remain significant
398 (Pillai's trace statistic, $F_{(5,16)}$=3.089, p=0.039) (Figure 2D), suggesting that $_{HEa}$miRNAs did not
399 mediate the effect of PAE in the rat model.

400 To determine if PAE-induced impairment of EMT in placenta is broadly conserved
401 throughout mammalian evolution, we adopted a non-human primate (macaque) model of
402 moderate to binge-type alcohol consumption. Placental tissues were isolated from GD85,
403 GD110, and GD 135 placenta (Figure 2E), which spans the human equivalent of mid- to second
404 mid-third trimester (Supplementary Figure 2C). There was a significant effect of ethanol
405 exposure on expression of EMT core genes by MANOVA (Pillai's trace statistic, $F_{(4,9)}$=4.229
406 p=0.045, Figure 3B). Consistent with our findings in mouse, post-hoc univariate ANOVA
407 indicated that in primate placenta, ethanol exposure significantly increased *CDH1* expression
408 ($F_{(1,12)}$=4.866, p=0.048) whereas *VIM* expression was significantly reduced ($F_{(1,12)}$=12.782,
409 p=0.0004), suggesting that, as in the mouse, PAE also impairs EMT in the primate placenta.
410 Interestingly, expression of *TWIST*, a pro-EMT transcription factor, was significantly increased
411 ($F_{(1,12)}$=5.31, p=0.04), though there was no effect on *SNAI2* expression (Figures 3G-3J). As in
412 mice, accounting for expression of $_{HEa}$miRNAs together as a covariate abolished the significant
413 effect of PAE on EMT, though to a greater degree than mice (Pillai's trace, $F_{(1,1)}$=1.605, p=0.425)
414 (Figure 2F). Interestingly, accounting for expression of individual $_{HEa}$miRNAs did not explain the
415 effects of PAE on placental EMT, suggesting that $_{HEa}$miRNAs act in concert to mediate the effect
416 of PAE on EMT in primate placenta (Figure 2G).
417 Collectively, our data suggests PAE induced impairment of EMT in the trophoblastic
418 compartment of placentae is conserved between rodents and primates and that $_{HEa}$miRNAs,
419 particularly in primates, may moderate the effect of PAE on placental EMT. Consequently,
420 subsequent studies focused on the collective role of $_{HEa}$miRNAs, either on basal or on alcohol-
421 influenced placental trophoblast growth, invasion, and the maturation of physiological function.

422 $_{HEa}$miRNAs impair the EMT pathway in cytotrophoblasts

423 To investigate whether $_{HEa}$miRNAs collectively interfere with the EMT pathway, as
424 suggested by our in vivo data, we measured expression of core members of the EMT pathway
425 after transfecting $_{HEa}$miRNA mimics and antagomirs into BeWO cytotrophoblasts.
426 Cytotrophoblasts normally undergo EMT to become invasive trophoblasts, which we also
427 modelled using the HTR8 human extravillous trophoblast cell line.
428 Transfection of pooled $_{HEa}$miRNAs into cytotrophoblasts significantly increased *CDH1* expression
429 ($F_{(1,36)}$=30.08, p<0.0001). Interestingly, expression of the pro-mesenchymal transcription factors
430 *TWIST* and *SNAI1* were also significantly reduced, but only in the context of concomitant 320
431 mg/dL ethanol treatment, pointing to an interaction effect between $_{HEa}$miRNAs and ethanol
432 ($F_{(1,36)}$= 5.650 and 5.146 respectively, p=0.023 and p=0.029) (Figures 4A-D). Consistent with our
433 qPCR data, transfection of $_{HEa}$miRNAs also significantly increased E-cadherin protein expression
434 ($F_{(1,20)}$=33.86, p<0.0001) (Figure 4E). We were unable to detect *SNAI2* transcript expression or
435 vimentin protein expression in these cells, consistent with previous reports (80).

436 Whereas transfection of $_{HEa}$miRNA mimics increased *CDH1* expression, transfection of
437 antagomirs significantly reduced CDH1 expression in the context of 320 mg/dL ethanol co-
438 exposure (Tukey's HSD, p=0.005), indicating an interaction effect ($F_{(1,36)}$=13.51, p=0.0008)
439 (Figure 4F). However, expression of *TWIST* was also decreased in this context and there was no
440 significant difference in E-Cadherin protein expression relative to the control (Figure 4G-J).
441 Thus, our data suggest that, increasing $_{HEa}$miRNA levels impairs EMT in cytotrophoblasts
442 whereas inhibiting their action has a more restricted effect on EMT pathway members.

443 $_{HEa}$miRNAs impair the EMT pathway in extravillous trophoblasts

444 We next investigated the effect of $_{HEa}$miRNAs on EMT in our extravillous trophoblasts.
445 Transfecting pooled $_{HEa}$miRNA mimics into extravillous trophoblasts significantly decreased *VIM*
446 expression ($F_{(1,36)}$=28.43, p<0.0001). Expression of pro-mesenchymal transcription factors *SNAI1*
447 and *SNAI2* was also reduced ($F_{(1,36)}$=27.30 and 64.88 respectively, p<0.0001). As with
448 cytotrophoblasts, expression of *TWIST* was reduced only with 320 mg/dL ethanol co-exposure
449 (Tukey's HSD, p =0.0273) indicating an interaction effect ($F_{(1,36)}$=5.184, p=0.029) (Figures 5A-D).
450 Consistent with our qPCR data, vimentin protein expression was also significantly reduced
451 ($F_{(1,20)}$=9.535, p=0.006) (Figure 5E). Interestingly, there was also a main effect of alcohol
452 exposure on decreasing vimentin protein expression ($F_{(1,20)}$=7.303, p=0.014). We were unable to
453 detect expression of *CDH1* transcript, or its E-Cadherin protein product, in extravillous
454 trophoblasts, consistent with previous reports(80).
455 In contrast to $_{HEa}$miRNA mimics, transfecting pooled antagomirs significantly increased
456 *VIM* expression ($F_{(1,35)}$=42.56, p<0.0001). Likewise, *SNAI1* and *SNAI2* were significantly
457 increased ($F_{(1,35)}$=18.43 and 27.02 respectively, p<0.0001), though there was no effect on *TWIST*
458 expression (Figures 5F-I). Despite our qPCR data, we did not observe significant differences in
459 vimentin protein expression between treatment groups. (Figures 5J). Collectively, our data
460 indicate that increased trophoblastic $_{HEa}$miRNA levels favors an epithelial phenotype, whereas
461 inhibiting their action promotes a mesenchymal phenotype.
462 <u>Antagomirs prevent $_{HEa}$miRNAs' inhibition of the EMT pathway</u>
463 We next investigated if pretreating trophoblasts with pooled $_{HEa}$miRNA antagomirs could
464 prevent inhibition of the EMT pathway caused by transfecting $_{HEa}$miRNA mimics. *CDH1*
465 expression in cytotrophoblasts transfected with control antagomir, and subsequently

466 transfected with control mimic, was not significantly different from those transfected with
467 $_{HEa}$miRNA antagomirs and $_{HEa}$miRNA mimics. However, *CDH1* was significantly elevated in
468 cytotrophoblasts transfected with control antagomir and $_{HEa}$miRNA mimics (Tukey's HSD, n=10
469 samples per group, p=0.004). Likewise, cells pre-transfected with $_{HEa}$miRNA antagomirs had
470 significantly higher *SNAI1* and *VIM* expression than those pre-transfected with control
471 antagomir and subsequently transfected with $_{HEa}$miRNA mimics (Tukey's HSD, n=10 samples per
472 group, p=0.007 and p<0.0001 respectively) (Figure 6A-D).
473 Furthermore, *VIM* expression in extravillous trophoblasts pre-transfected with control
474 antagomir, and subsequently transfected with control mimic, was not significantly different
475 from those transfected with $_{HEa}$miRNA antagomirs and $_{HEa}$miRNA mimics. However, *VIM*, *SNAI1*,
476 and *SNAI2* expression were significantly reduced in cytotrophoblasts transfected with control
477 antagomir and $_{HEa}$miRNA mimics (Tukey's HSD, n=10 samples per group, p<0.0001) (Figure 6E-
478 H). Thus, our data suggest that pretreating cells with $_{HEa}$miRNA antagomirs prevents the EMT
479 pathway inhibition resulting from transfection with $_{HEa}$miRNA mimics in cytotrophoblasts and
480 extravillous trophoblasts.
481 <u>$_{HEa}$miRNAs impair extravillous trophoblast invasion</u>
482 Functionally, inhibition of the EMT pathway should reduce trophoblast invasiveness.
483 Thus, we performed a transwell invasion assay using extravillous trophoblasts transfected with
484 $_{HEa}$miRNA mimics and antagomirs. While ethanol exposure by itself did not impair trophoblast
485 invasion (Supplementary Figure 5), a planned comparison demonstrated significantly reduced
486 invasiveness of trophoblasts transfected with $_{HEa}$miRNA mimics relative to the control mimics in
487 the context of 320 mg/dL ethanol co-exposure (t(14)=2.762, p=0.015), consistent with our data

488 that elevated $_{HEa}$miRNAs inhibit the EMT pathway (Figure 7A). Contrastingly, transfecting
489 $_{HEa}$miRNA antagomirs increased invasion in the context of 320 mg/dL ethanol co-exposure,
490 though this effect was only marginally significant (t(14)=1.805, p=0.093) (Figure 7B).

491 <u>$_{HEa}$miRNAs retard trophoblast cell cycle progression</u>

492 Given the proliferative nature of cytotrophoblasts, and the intimate relationship
493 between EMT and cell cycle (81, 82), we assessed the effects of ethanol and $_{HEa}$miRNAs on
494 BeWO cytotrophoblast cell cycle. After pulse-labeling cells with EdU for 1-hour, we found that
495 individually transfecting 6 of the $_{HEa}$miRNA mimics increased EdU incorporation (Unpaired t-
496 test, $p<0.05$, FDR correction), suggesting an overall increased rate of DNA synthesis
497 (Supplementary Figure 6A). Contrastingly, simultaneous transfection of $_{HEa}$miRNAs significantly
498 reduced the degree of EdU incorporation($F_{(1,26)}=59.69$, $p<0.0001$), mirroring the effects of
499 increasing concentrations of ethanol ($R^2=0.304$, p=0.012) (Supplementary Figure 6B and Figure
500 8A).

501 Consistent with the increased rates of DNA synthesis resulting from individual $_{HEa}$miRNA
502 mimic transfection, individual transfection of $_{HEa}$miRNAs antagomirs generally reduced EdU
503 incorporation, though only the antagomir to hsa-miR-760 did so significantly (t(110)=3.059,
504 p=0.003, FDR correction) (Supplementary Figure 6A). Interestingly, simultaneous administration
505 of antagomirs also reduced EdU incorporation similar to the pooled $_{HEa}$miRNAs mimics
506 ($F_{(1,26)}=34.83$, p=0.0005) (Figure 8B).

507 To further characterize the coordinated effect of $_{HEa}$miRNAs on cytotrophoblast cell
508 cycle, we pulsed cells with EdU for 1-hour and, post-fixation, labelled them with 7AAD to
509 segregate cells into three groups: G_0/G_1 (7AADlow, EDU-), S (EDU+), and G_2/M (7AADhigh, EDU-

510). Both 120 mg/dL and 320 mg/dL ethanol exposures significantly decreased the proportion of
511 cells in S-phase, while 320 mg/dL exposure increased the proportion of cells in G_2/M-phase,
512 consistent with the observed reduction in the rate of DNA synthesis (Supplementary Figures
513 6C). Similar, to the effects of ethanol exposure, pooled $_{HEa}$miRNA mimic administration also
514 significantly decreased the proportion of cells in S-phase ($F_{(1,28)}$=52.78, p<0.0001) while
515 increasing the proportion of cells the G_2/M-phase ($F_{(1,28)}$=8.395, p=0.007) and exacerbated
516 alcohol's effects on the cell cycle (Figure 8C). Interestingly, pooled $_{HEa}$miRNA antagomir
517 administration also reduced the proportion of cells in S-phase ($F_{(1,26)}$=14.98, p=0.0007) and
518 increased the proportion of those in G_2/M-phase ($F_{(1,26)}$=12.38, p=0.002), though this effect was
519 only significant when cells were also exposed to 320 mg/dL ethanol (Tukey's HSD, p=0.011)
520 (Figure 8D).

521 We sought to determine if pretreating cytotrophoblasts with pooled $_{HEa}$miRNA
522 antagomirs could prevent the cytotrophoblast cell cycle retardation caused by transfecting
523 $_{HEa}$miRNA mimics. Cells transfected with the control or pooled $_{HEa}$miRNA antagomirs, and
524 subsequently transfected with pooled $_{HEa}$miRNA mimics, did not have significantly different cell
525 cycle profiles or rates of DNA synthesis to each other but had significantly lower rates of DNA
526 synthesis (ANOVA, $F_{(2,12)}$=16.56, p=0.0004), and a decreased proportion of S-phase cells
527 ($F_{(2,12)}$=11.43, p=0.002) with an increased proportion of cells in G_2/M phase ($F_{(2,12)}$=11.47,
528 p=0.002), compared to cells transfected with both the control antagomir and control mimic
529 (Figures 9A and B). Collectively, our data indicate that transfection of these antagomirs
530 prevents further reduction in the rate of DNA synthesis, or cell cycle retardation, that would
531 result from pooled $_{HEa}$miRNA mimic transfection.

532 $_{HEa}$miRNAs have minimal effect on cell survival

533 We next sought to investigate whether ethanol- and $_{HEa}$miRNA-induced changes in cell
534 cycle were related to an increase in cell death. Only the 320 mg/dL dose of ethanol exposure
535 demonstrated a slight, but marginally significant effect, of increasing lytic cell death
536 ($t(18)=2.022$, $p=0.054$), though there was no effect on apoptosis (Supplementary Figures 6A and
537 B). However, the changes in cell cycle following transfection of individual or pooled $_{HEa}$miRNA
538 mimics were not mirrored by changes in lytic cell death. Nevertheless, two $_{HEa}$miRNAs, hsa-mir-
539 671-5p and hsa-mir-449a, did significantly increase apoptosis (Unpaired t-test, $p<0.05$, FDR
540 correction) (Supplementary Figures 6C and D).

541 Contrastingly, transfection of 4 $_{HEa}$miRNA antagomirs significantly increased lytic cell
542 death (Unpaired t-test, $p<0.05$, FDR correction) with the antagomir to hsa-mir-491-3p also
543 increasing apoptotic cell death ($t(14)=3.383$, $p=0.004$, FDR correction) (Supplementary Figure
544 6C and D). Likewise, transfection of pooled $_{HEa}$miRNA antagomirs increased lytic cell death
545 ($F_{(1,36)}=11.40$, $p=0.002$) but did not cause increased apoptosis (Supplementary Figure 6E-H).
546 Taken together, our data suggest that while ethanol exposure may increase cytotrophoblast
547 death, increased levels of $_{HEa}$miRNAs have minimal effects on cell death, suggesting that their
548 effect on cell cycle and the EMT pathway is independent of any effect on cell survival.

549 $_{HEa}$miRNAs modulate cytotrophoblast differentiation-associated Ca^{2+} dynamics

550 Inhibition of the EMT pathway, coupled with cell cycle retardation, indicates that
551 $_{HEa}$miRNAs influence trophoblast maturation. Maturation of cytotrophoblasts into
552 syncytiotrophoblasts is marked by dramatic changes in the cellular energetics profile. In order
553 to model $_{HEa}$miRNAs' effect on hormone-producing syncytiotrophoblasts, we used a well-

554 established protocol of forskolin induced syncytialization of BeWO cytotrophoblasts. As
555 expected, forskolin treatment induced fusion/syncytialization of cytotrophoblasts resulting in a
556 greater average cell size in the forskolin + $_{HEa}$miRNA mimics group ($F_{(1,386)}$=4.386, p=0.037). This
557 suggests that the inhibition of EMT by these miRNAs may result in preferential syncytialization
558 instead of differentiation to extravillous trophoblasts (Supplementary Figure 5A). Ethanol and
559 forskolin treatment both increased baseline calcium levels, as indicated by the change in fluo-4
560 fluorescence ($F_{(1,426)}$=5.593 and 3.665 respectively, p<0.0001) (Figure 10A, Supplementary
561 Figures 5B-D). The effect of ethanol on baseline calcium was abrogated by $_{HEa}$miRNAs while
562 $_{HEa}$miRNAs + forskolin was not significantly different to forskolin alone, indicating that forskolin
563 and $_{HEa}$miRNAs may be affecting similar calcium pathways. Syncytiotrophoblasts actively
564 transport high amounts of calcium from maternal to fetal circulation, therefore forskolin-
565 exposed trophoblasts likely have higher basal transport of calcium into the cells due to
566 increased expression of plasma membrane channels (83). The conversion of trophoblasts to
567 synciotrophoblasts is accompanied by an increase in endoplasmic reticulum(84), which could
568 increase calcium buffering capabilities in response to ethanol-stress on the cells, thus $_{HEa}$miRNA-
569 induced syncytialization pathways may be protective against ethanol stress.
570 Adaptations to cellular stress can be seen in alterations to cellular energetics in
571 response to ethanol, as ethanol-exposed BeWO cells showed decreased baseline and stressed
572 oxygen consumption rates (OCR) ($F_{(1,28)}$=15.55 and 16.91, p=0.0005 and 0.0003 respectively)
573 and increased extracellular acidification rates (ECAR) ($F_{(1,28)}$=4.868, p=0.036). However,
574 $_{HEa}$miRNAs had minimal effects on metabolic activity (Figures 10D-10G).

575 Extracellular ATP has been shown to inhibit trophoblast migration (85) and can directly
576 stimulate increased intracellular calcium elevations through purinergic receptors ubiquitously
577 present on trophoblasts (86). Both $_{HEa}$miRNA and ethanol administration significantly increased
578 intracellular calcium in response to acute ATP administration ($F_{(1,426)}$=10.34 and $F_{(1,386)}$=16.30,
579 p=0.001 and p<0.0001 respectively) (Figure 10B). This may be indicative of a lack of
580 downregulation of purinergic receptors required in trophoblast migration as part of the
581 interrupted EMT pathway. Forskolin-induced maturation decreased calcium response to ATP
582 ($F_{(1,386)}$=50.72, p<0.0001) (Figure 10C) and prevented the $_{HEa}$miRNA-induced increase in ATP
583 response. These data agree with previous studies showing increased nuclear trafficking of
584 ionotropic receptor P2X7 and more localized P2X4 expression over placental development,
585 which may decrease the overall calcium influx in response to ATP (87).

586 $_{HEa}$miRNAs promotes syncytialization-dependent hormone production

587 Transfection of $_{HEa}$miRNA mimics did not change *CGA*, *CGB*, or *IGF2* transcript expression
588 relative to the control in non-syncytialized trophoblasts. However, following syncytialization,
589 $_{HEa}$miRNA mimics significantly increased expression of *CGA* and *CGB* (Tukey's HSD, n=10 samples
590 per group, p=0.001 and 0.005 respectively). Consistent with our previous results, $_{HEa}$miRNA
591 mimics also increased *CDH1* expression in both cytotrophoblasts and syncytiotrophoblasts
592 ($F_{(1,20)}$=5.286, p=0.032); there was also a main effect of syncytialization on *CDH1* expression, as
593 has been previously reported ($F_{(1,36)}$=3.391, p=0.034) (Figures 11A-D). Likewise, $_{HEa}$miRNAs
594 increased E-cadherin protein expression ($F_{(1,20)}$=5.286, p=0.032), whereas forskolin decreased it
595 ($F_{(1,20)}$=10.24, p=0.005) (Figure 11E). On the other hand, there was no effect of $_{HEa}$miRNA
596 antagomirs on *CGA* and *CGB* expression, although we did observe a decrease in *IGF2* transcript

597 expression, following syncytialization, relative to controls (Tukey's HSD, n=10 samples per
598 group, p=0.001) (Figure 11F-I).

599 Given that $_{HEa}$miRNAs promotes syncytialization-dependent hormone production, we
600 next investigated maternal plasma levels of intact human chorionic gonadotropin (hCG) in our
601 Ukraine birth cohort. Plasma hCG levels were non-significantly increased in the second
602 trimester of HEa group mothers relative to their UE counterparts, consistent with previous
603 studies (88). During the third trimester, however, hCG levels remained significantly elevated in
604 HEa group mothers compared to the UE group (Median Test(89), n=23 samples in HEa group
605 and n=22 for HEua and HEa groups, p=0.03) (Figure 12). Furthermore, there was no significant
606 difference of gestational age at blood draw between the different groups indicating the
607 increased level of hCG in the HEa group was not confounded by gestational age at which blood
608 was sampled (Supplementary Figure 8) (90) . Interestingly, both alcohol and hCG levels were
609 negatively associated with gestational age at delivery (GAD), with a significant interaction
610 between periconceptional alcohol exposure and hCG levels on GAD (Supplementary Table 3).
611 Taken together, our data suggests $_{HEa}$miRNAs may contribute to PAE-dependent increases in
612 hCG levels during pregnancy.

613 <u>$_{HEa}$miRNAs reduce fetal growth</u>

614 To investigate the functional consequences of elevated circulating $_{HEa}$miRNA levels, we
615 administered miRNA mimics for the 8 mouse homologue $_{HEa}$miRNAs, or a negative control
616 mimic, through tail-vein injection to pregnant mouse dams on GD10. On GD18, growth
617 parameters of male and female fetuses were assessed separately, and data from all same-sex
618 fetuses from a single pregnancy were averaged into one data point. Dams administered

619 $_{HEa}$miRNA mimics produced smaller fetuses than those administered control mimics, according

620 to all collected measures of fetal size: fetal weight ($F_{(1,17)}$=13.78, p=0.002), crown-rump length

621 ($F_{(1,17)}$=14.15, p=0.002), snout-occipital distance ($F_{(1,17)}$=8.032, p=0.012), and biparietal diameter

622 ($F_{(1,17)}$=6.371, p=0.022) (Figure 13B-E). Interestingly, placental weights were also significantly

623 reduced in mice treated with $_{HEa}$miRNA mimics ($F_{(1,17)}$=5.784, p=0.0278) (Figure 13F).

624

625 **Discussion**

626 In a prior study, we reported that gestational elevation of 11 maternal plasma miRNAs,
627 in a Ukrainian clinical cohort, predicted which PAE infants would exhibit adverse outcomes at
628 birth (11). These $_{HEa}$miRNAs were elevated throughout mid and late-pregnancy, encompassing
629 critical periods for fetal development, and were predicted to target key developmental
630 pathways (11). Given that $_{HEa}$miRNAs are placentally enriched and their dysregulation is
631 associated with placental-associated gestational pathologies, we sought to determine if they
632 also contributed to the pathophysiology of FASDs.

633 In order to mimic the alcohol consumption patterns in our Ukrainian cohort, we
634 adopted moderate alcohol self-administration paradigms during mouse, rat, and macaque
635 gestation. Though these species share a hemochorial placenta, fundamental differences in
636 placental anatomy remain. Specifically, macaque and rat extravillous trophoblasts exhibit
637 deeper invasion into the uterine horn than their mouse counterparts (91-94). Our models also
638 differed on the duration of ethanol exposure as well as the timepoints of placental harvest. In
639 our rat model, PAE was restricted to a periconceptional period, while PAE was more
640 longitudinal in our mouse and primate models. Additionally, the GD20 timepoint of placental
641 harvest in rats corresponds to a period where trophoblast invasion is completed and
642 mesometrial regression is occurring, whereas trophoblast invasion is only initiating during the
643 GD14 placental harvest timepoint in mice (93, 95). Despite these differences, we found PAE
644 inhibited mesenchymal transition-associated mRNA transcripts in all our models, indicating a
645 strong and persistent effect of PAE on placental development. Additionally, we found that
646 $_{HEa}$miRNAs mediated the effects of PAE on placental EMT, and collectively though not

647 individually, inhibited EMT in human cytotrophoblast and extravillous trophoblast culture
648 models.

649 Interestingly, $_{HEa}$miRNAs also promoted syncytialization (forskolin)-dependent hCG
650 expression, mirroring the elevation of third trimester maternal hCG levels in the PAE group
651 within our Ukrainian birth cohort. This late-gestation elevation of hCG levels may serve as a
652 compensatory mechanism to prevent the preterm birth associated with PAE, as hCG during late
653 gestation is hypothesized to promote uterine myometrial quiescence (96, 97). In support of this
654 hypothesis, we found significant negative associations between both hCG levels and alcohol
655 consumption with gestational age at delivery. Furthermore, there was a significant interaction
656 between periconceptional alcohol exposure and hCG levels, with higher hCG levels
657 corresponding to a smaller effect of alcohol exposure at conception on gestational age at
658 delivery, indicating that hCG moderates the effect of alcohol on age at delivery (Supplementary
659 Table 3).

660 Since $_{HEa}$miRNAs collectively prevented trophoblast EMT, we hypothesized that, as a
661 functional consequence, these maternal miRNAs would also inhibit fetal growth. When we
662 delivered 8 out of the 11 $_{HEa}$miRNAs known to be present in mouse, to pregnant dams during
663 the period of placental branching morphogenesis and endometrial invasion (31), when EMT is
664 particularly active, we found that $_{HEa}$miRNAs reduced fetal growth. Importantly, ethanol
665 exposure during this period has also been shown to result in fetal growth deficits and
666 dysmorphia in rodent PAE models (98, 99) suggesting that maternal miRNA-mediated deficits in
667 trophoblast invasion may mediate some of the effects of PAE on fetal growth. It is feasible that
668 $_{HEa}$miRNAs disrupt fetal growth through placental vascular dynamics. The non-human primate

669 tissue analyzed here was derived from animals that were characterized in vivo using MRI and
670 ultrasound imaging, which demonstrated that maternal blood supply to the placenta was lower
671 in ethanol-exposed animals compared to controls, and that oxygen availability to the fetal
672 vasculature was reduced (33). Thus, one possibility is that compromised trophoblast invasion
673 contributes to impaired maternal blood flow in ethanol-exposed individuals, as we have also
674 previously observed in mouse models (100).

675 Impaired nutrient uptake in the placenta, such as dysfunction in the amino acid, glucose,
676 and fatty acid transport systems have also been implicated in gestational pathologies, such as
677 intrauterine growth restriction (101). Furthermore, in vitro studies in trophoblasts have shown
678 alcohol exposure selectively impairs a subset of these amino acid and fatty acid transport
679 systems (102, 103) whilst in vivo, our rat model of exposure around conception alters
680 expression of glucose transporters in the late gestation placenta (23). These placental
681 dysfunctions could also have insidious effects on development that are not immediately
682 detectable at birth. As an example, perturbations in placental iron transport by PAE may impair
683 central nervous system development during the neonatal period, leading to cognitive deficits
684 that last throughout adulthood(104, 105). Thus, further investigation is warranted to determine
685 if $_{HEa}$miRNAs contribute to this alcohol induced impairment in trans-placental nutrient
686 transport, and ultimately whether or not this impairment of nutrient transport represents
687 another avenue through which PAE disrupts fetal development.

688 It is likely that $_{HEa}$miRNAs may mediate other pregnancy associated pathologies, aside
689 from PAE. We identified a number of studies that reported increased circulating and placental
690 levels of at least 8 out of 11 $_{HEa}$miRNAs in gestational pathologies arising from placental

691 dysfunction. For example, elevated levels of one $_{HEa}$miRNA, miR-519a-3p, a member of the
692 placentally-expressed C19MC family cluster, was reported in placentae of patients with pre-
693 eclampsia, recurrent spontaneous abortion, and intrauterine growth restriction (52, 53, 66, 67).
694 Interestingly, collective overexpression of the 59 C19MC miRNAs inhibits trophoblast migration,
695 explaining their enrichment in the non-migratory villous trophoblasts and suggests their
696 downregulation is necessary for maturation into invasive extravillous trophoblasts (106). Thus,
697 a greater understanding of the placental roles of $_{HEa}$miRNAs may also help disentangle the
698 etiology of other pregnancy complications.

699 While our data suggest that the placenta is an important contributory source for
700 circulating $_{HEa}$miRNAs, the effects of $_{HEa}$miRNAs likely extend beyond the placenta into other
701 maternal tissues. Outside of the placenta, $_{HEa}$miRNAs may circulate in association with
702 lipoprotein complexes, or be encapsulated in extracellular vesicles (EVs) whose abundance
703 dramatically increases during pregnancy (107, 108).Recent work has demonstrated that
704 placental-derived EVs can regulate the maternal immune system as well as confer viral
705 resistance to recipient cells, including endothelial cells (109-112). Interestingly, other studies
706 also have identified endothelial cells as ready recipients for placental-derived EVs, suggesting
707 placental-EVs and their cargo miRNAs participate in synchronizing the growth of the placenta
708 with the accompanying maternal and fetal vascular remodeling (107, 113). While further
709 investigation is warranted into the role of EVs and miRNAs in maternal-fetal communication,
710 and to the extent they serve as paracrine/endocrine mediators for the placenta during
711 development, targeting $_{HEa}$miRNAs will likely have profound effects for both fetal and placental
712 development in the context of FASDs and other gestational pathologies.

713 While we did not investigate the effects of PAE on EMT in non-placental organs, it is
714 likely that PAE broadly disrupts EMT in multiple fetal compartments. Developmental ethanol
715 exposure has been shown inhibit the EMT-dependent migration of neural crest progenitors
716 involved in craniofacial development, explaining the facial dysmorphology seen in FAS and
717 FASDs (114, 115). Outside of its effects on the neural crest, PAE is significantly associated with
718 various congenital heart defects, including both septal defects and valvular malformations (116-
719 119). Septation of the heart, primarily atrial septation, is an EMT-dependent process, with
720 endocardial cells delaminating and transdifferentiating into mesenchymal cells that populate
721 the endocardial cushions as well as the muscular cap, which functions as the growing edge of
722 the muscular atrial septum(120, 121). The mesenchymal cells from the endocardial cushions
723 also form the cardiac valve progenitors. Thus, disruption of endocardial EMT could explain both
724 the valvular and septal malformation associated with PAE.
725 Collectively, our data on $_{HEa}$miRNAs suggest miRNA-based intervention could minimize
726 or reverse developmental effects of PAE and other placental-related pathologies. miRNA-based
727 therapeutic approaches have been advanced for other disease conditions. For example,
728 Miraversen^{tm}, an anti-miR-122 antisense oligonucleotide, has been shown to be effective in
729 reducing hepatitis-C viral burden (122). Additionally, a recent phase-1 clinical trial report
730 indicated that liposomal delivery of a tumor-suppressor miRNA was well tolerated in human
731 populations and showed evidence of therapeutic efficacy (123). However, we also observed
732 with $_{HEa}$miRNAs that the effects of combinations of miRNAs are not a sum of their individual
733 effects. Functional synergy between clusters of co-regulated miRNAs may be a common feature
734 in development and disease. For instance, in 2007, we presented early evidence that ethanol

735 exposure reduced miR-335, -21, and -153 in neural progenitors and that coordinate reduction
736 in these miRNAs yielded net resistance to apoptosis following ethanol exposure (124). In that
737 study, we also showed that coordinate knockdown of these three miRNAs was required to
738 induce mRNA for Jagged-1, a ligand for the Notch cell signaling pathway, an outcome that was
739 not recapitulated by knocking down each miRNA individually (124). More recently, combined
740 administration of miR-21 and miR-146a has been shown to be more effective in preserving
741 cardiac function following myocardial infarction than administration of either of these miRNAs
742 alone (125). While miRNA synergy has not been explored in detail, these data show that new
743 biology may emerge with admixtures of miRNAs, and that therapeutic interventions may
744 require the use of such miRNA admixtures rather than single miRNA molecules as have been
745 used in clinical studies to date. Our study was restricted to exploring the effects of the 11
746 $_{HEa}$miRNAs on development, which represent only the significantly increased fraction of miRNAs
747 elevated in the HEa group maternal plasma within our Ukrainian cohort. Indeed, the next 5
748 most elevated miRNAs are also abundantly expressed in the placenta (data not shown),
749 indicating they may also mediate the effects of PAE on placental biology.
750 In conclusion, we have observed how a set of 11 miRNAs, predictive of adverse infant
751 outcomes following PAE, collectively mediate the effects of alcohol on the placenta. Specifically,
752 elevated levels of these miRNAs promote an aberrant maturational phenotype in trophoblasts
753 by inhibiting the EMT pathway and promoting syncytialization-dependent hormone production.
754 Functionally, these miRNAs are clinically correlated with measures of fetal development and
755 directly cause intrauterine growth restriction when administered in vivo. Our work suggests
756 that a greater understanding for the role of $_{HEa}$miRNAs during development, and their role in

757 coordinating the EMT pathway in the placenta and other developing tissues, will benefit the
758 understanding of FASDs and other gestational pathologies and potentially lead to effective
759 avenues for intervention.

Figures

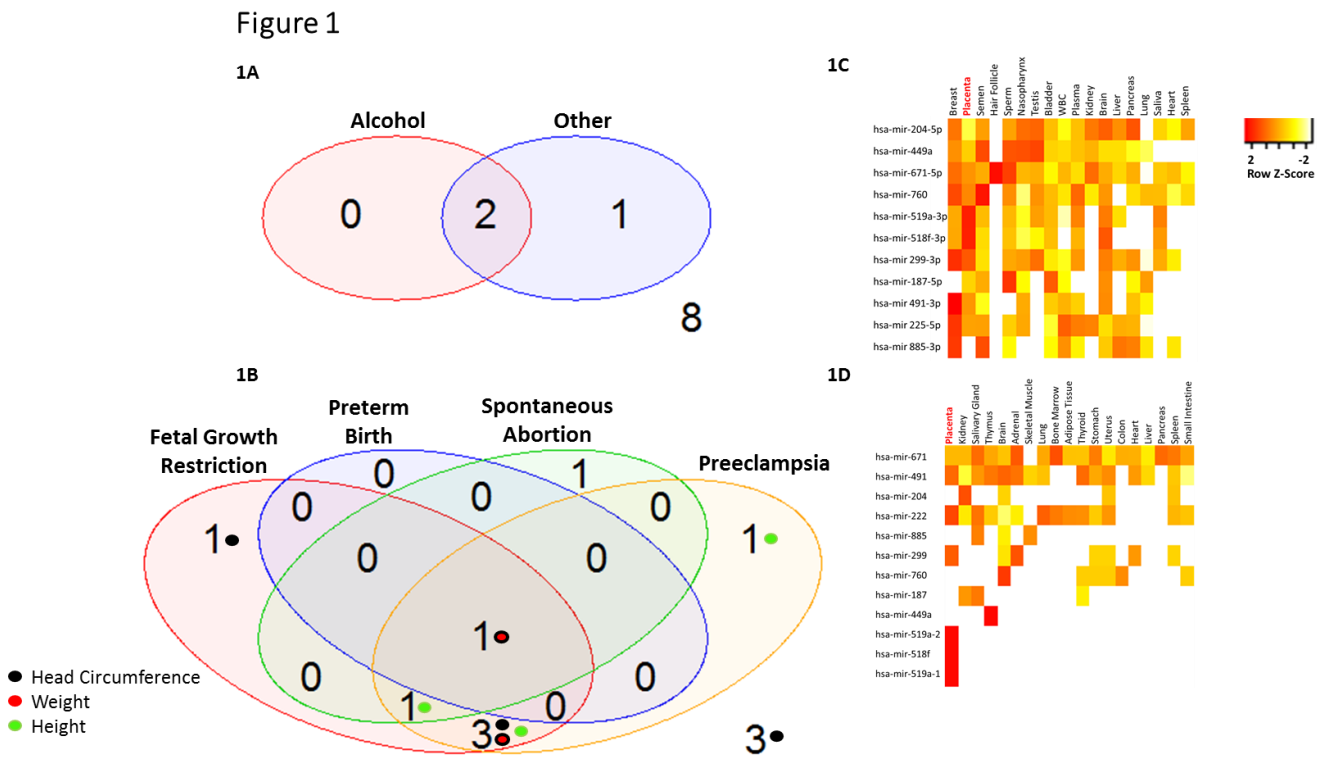

Figure 1: $_{HEa}$miRNAs are placentally enriched and associated with gestational pathologies

1A) Venn diagram on number of $_{HEa}$miRNAs reported to be associated with alcohol or other prenatal exposures.

1B) Venn diagram on number of $_{HEa}$miRNAs reported to be associated with different gestational pathologies. Inset colored circles the corresponding sex and gestational age-adjusted growth parameters these miRNAs were correlated with.

1C) Heatmap of mature $_{HEa}$miRNA expression and 1D) pri-$_{HEa}$miRNA expression across different tissues resulting from secondary analysis of publicly available RNA-sequencing data. Legend depicts row-centered Z-score.

Figure 2

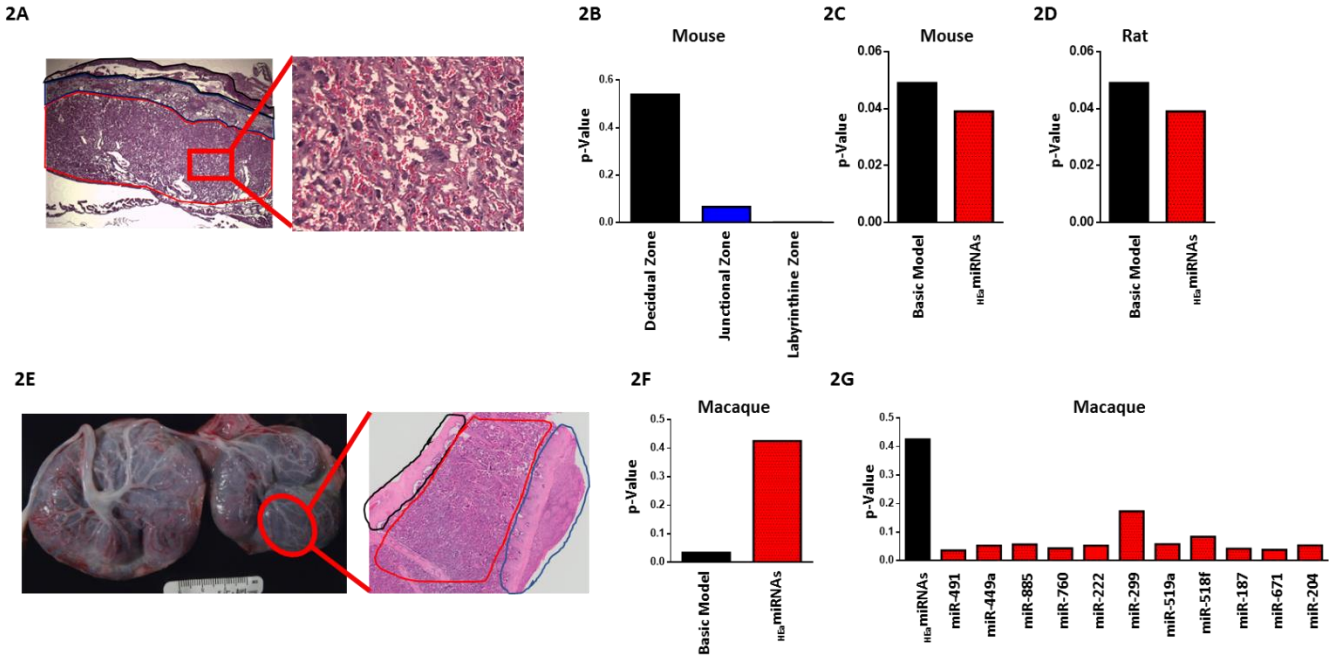

Figure 2: $_{HEa}$miRNAs mediate the effect of PAE on the EMT pathway in mouse and macaque placentas.

2A) Histological image of GD14 mouse placenta. Outlined in red is the labyrinth zone, blue is the junctional zone, black is the decidual zone. Inset is a high magnification image of the labyrinth zone.
2B) MANOVA of gene expression of core EMT pathway members in different regions of the mouse placenta in control and PAE mice (n=29 samples).
2C) MANCOVA of gene expression of core EMT pathway members in the mouse placental labyrinth zone before (Basic Model) and after accounting for the expression of $_{HEa}$miRNAs (n=29 samples).
2D) MANCOVA of gene expression of core EMT pathway members in the rat placental labyrinth zone before (Basic Model) and after accounting for the expression of $_{HEa}$miRNAs (n=32 samples).
2E) Gross anatomy photograph of the primary (left) and secondary (right) lobes of a GD135 macaque placenta. Outlined in red is an individual cotyledon from the secondary lobe. Inset is a full thickness hematoxylin and eosin stained histological section of a representative cotyledon with the fetal membranes outlined in black, villous tissue outlined in red and maternal decidua in blue.
2F) MANCOVA of gene expression of core EMT pathway members in placental cotyledons of PAE and control macaques, accounting for the expression of $_{HEa}$miRNAs collectively (n=23 samples).
2G) MANCOVA of gene expression of core EMT pathway members in macaque placentas after accounting for expression of $_{HEa}$miRNAs individually (n=23 samples).

Figure 3

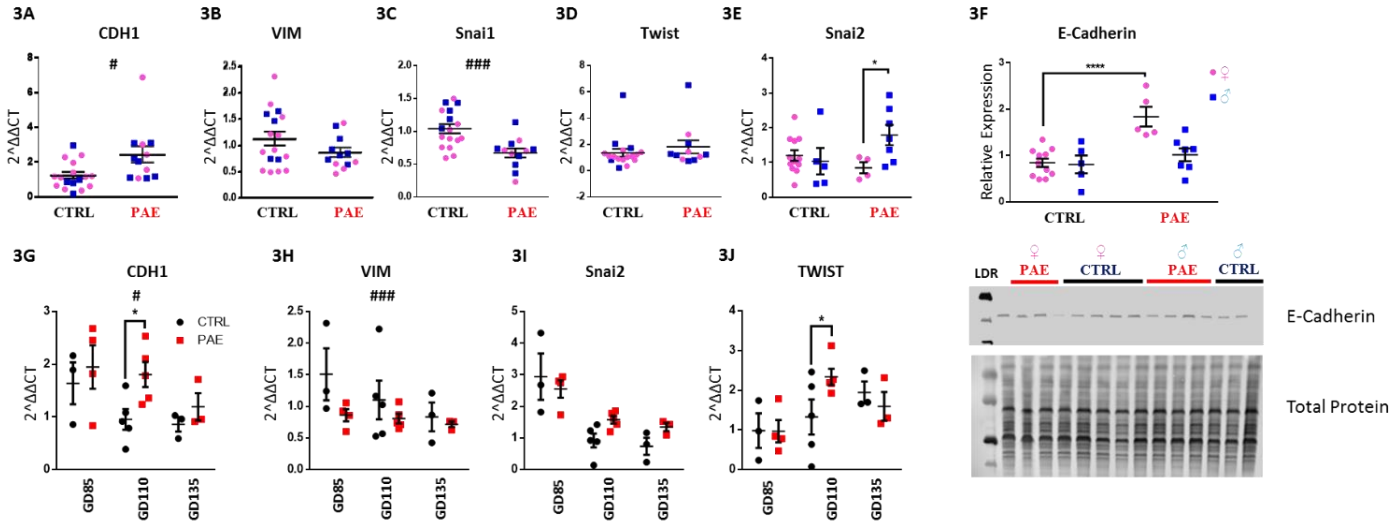

Figure 3: PAE impairs EMT in mouse and macaque placentas

Expression of 3A) *CDH1*, 3B) *VIM*, 3C) *SNAI1*, 3D) *TWIST*, and 3E) *SNAI2* in the placental labyrinth zone of PAE and control mice (n=5-12 samples per group).

3F) Densitometric quantification of E-Cadherin expression in the labyrinth zone of PAE and control mice as well as representative blot of E-Cadherin expression (top) and total protein expression (bottom, n=5-12 samples per group).

Expression of 3G) *CDH1*, 3H) *VIM*, 3I) *SNAI2*, and 3J) *TWIST* transcripts in PAE and Control macaque placental cotyledons (n=3-5 samples per group).

LDR=Molecular Weight Ladder; $^{\#}p<0.05$, $^{\#\#\#}p<0.001$, main effect by ethanol exposure; $^{*}p<0.05$ $^{***}p<0.001$, $^{****}p<0.00001$ by Tukey's HSD. Transcripts with a significant interaction between ethanol exposure and sex are plotted disaggregated by sex.

Figure 4

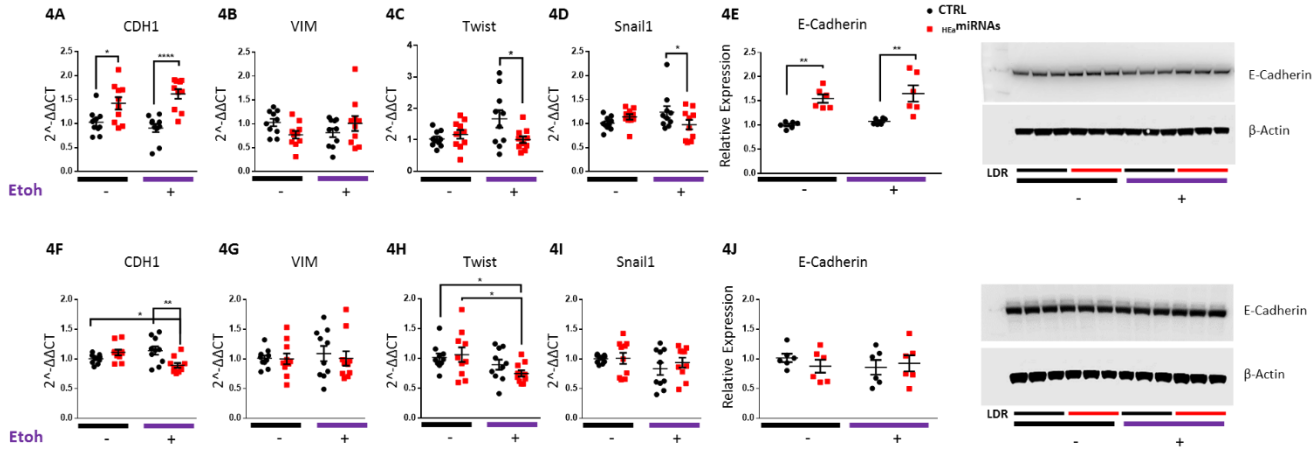

Figure 4: $_{HEa}$miRNAs impairs EMT in BeWO cytotrophoblasts

Expression of 4A) *CDH1,* 4B) *VIM,* 4C) *TWIST,* and 4D) *SNAI1* transcripts 4E) and densitometric quantification of E-Cadherin protein levels in BeWO cytotrophoblasts following $_{HEa}$miRNAs or control miRNA overexpression with or without concomitant 320 mg/dL ethanol exposure. 4F) Expression of *CDH1,* 4G) *VIM,* 4H) *TWIST,* and 4I) *SNAI1* transcripts 4J) and densitometric quantification of E-Cadherin protein levels in BeWO cytotrophoblasts following $_{HEa}$miRNAs or control hairpin inhibitor transfection with or without concomitant 320 mg/dL ethanol exposure. LDR=Molecular Weight Ladder, N=10 samples per group, *p<0.05, **p<0.01, ****p<0.0001 by Tukey's HSD.

Figure 5

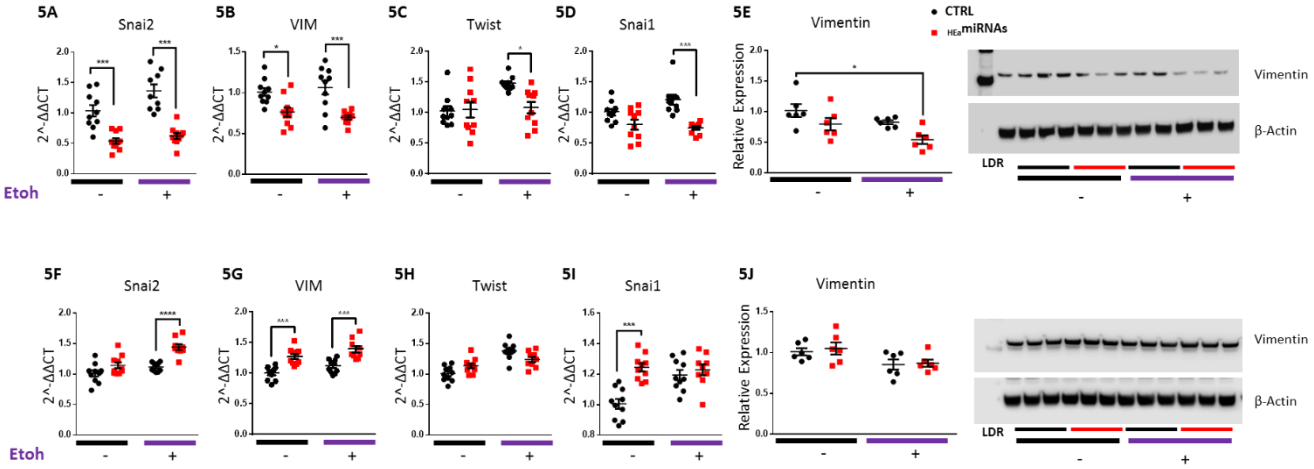

Figure 5: $_{HEa}$miRNAs impairs EMT in HTR8 extravillous trophoblasts

Expression of 5A) *CDH1* 5B) *VIM* 5C) *TWIST* and 5D) *SNAI1* transcripts 5E) as well as densitometric quantification of Vimentin protein levels in HTR8 extravillous trophoblasts following $_{HEa}$miRNAs or control miRNA overexpression with or without concomitant 320 mg/dL ethanol exposure.

Expression of 5F) *CDH1* 5G) *VIM* 5H) *TWIST* and 5I) *SNAI1* transcripts 5J) as well as densitometric quantification of Vimentin protein levels in HTR8 extravillous trophoblasts following $_{HEa}$miRNA or control hairpin inhibitor transfection with or without concomitant 320 mg/dL ethanol exposure.

LDR=Molecular Weight Ladder, N=10 samples per group, *p<0.05, ***p<0.001,****p<0.0001 by Tukey's HSD.

Figure 6

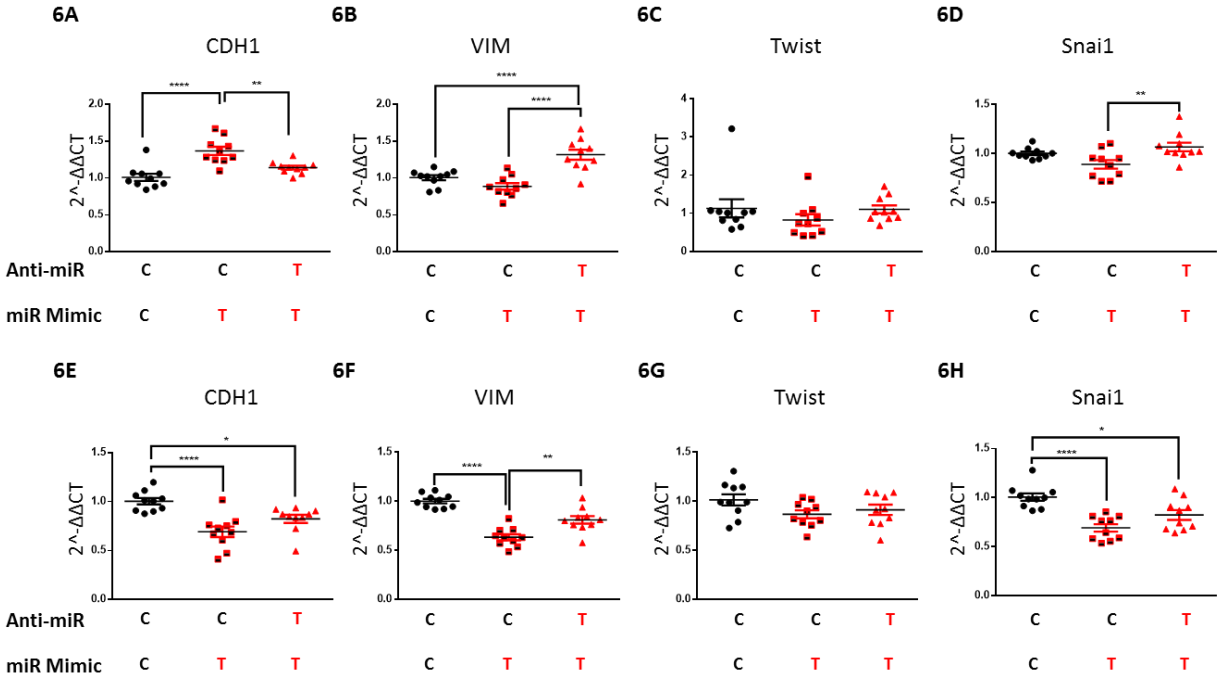

Figure 6: Antagomirs prevent $_{HEa}$miRNA induced impairment of EMT

Expression of 6A) *CDH1* 6B) *VIM* 6C) *TWIST* and 6D) *SNAI1* Transcripts following control or $_{HEa}$miRNA hairpin inhibitor transfection followed by control or $_{HEa}$miRNA overexpression in BeWO cytotrophoblasts.

Expression of 6E) *CDH1* 6F) *VIM* 6G) *TWIST* and 6H) *SNAI1* Transcripts following control or $_{HEa}$miRNA antagomir transfection followed by control or $_{HEa}$miRNA overexpression in HTR8 extravillous trophoblasts.

In subheadings: **C** denotes control miRNA mimic or hairpin whereas **T** denotes $_{HEa}$miRNA mimic or hairpin inhibitor. N=10 samples per group, *p<0.05, LDR=Molecular Weight Ladder, ***p<0.001, ****p<0.0001 by Tukey's HSD.

Figure 7

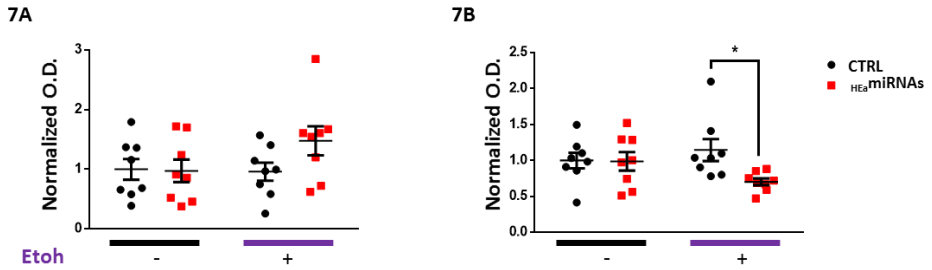

843
844 **Figure 7: $_{HEa}$miRNA impair extravillous trophoblast invasion**
845 Transwell invasion of HTR8 extravillous trophoblasts following transfection with 7A) $_{HEa}$miRNA
846 mimics or 7B) hairpin inhibitors with or without concomitant 320 mg/dL ethanol exposure.
847 N=10 samples per group, *p<0.05 by Unpaired T-test
848

Figure 8

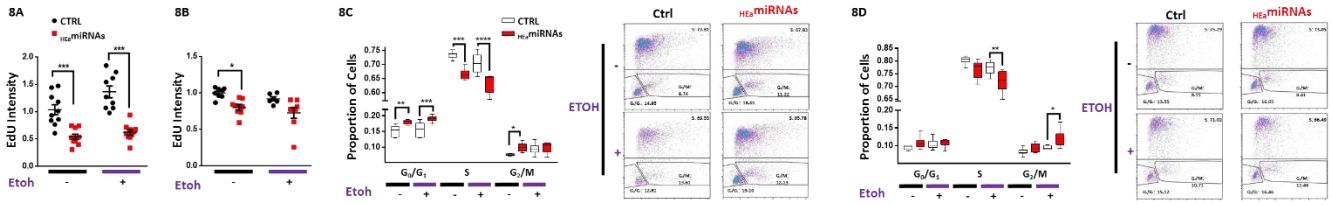

Figure 8: $_{HEa}$miRNA cause cell cycle retardation in trophoblasts

8A) Degree of EdU incorporation following control and $_{HEa}$miRNA overexpression or 8B) control and $_{HEa}$miRNA hairpin inhibitor transfection with or without concomitant 320 mg/dL ethanol exposure in BeWO cytotrophoblasts.

8C) Box and whisker plot for the proportion of cells in G_0/G_1, S, or G_2/M phase of the cell cycle following control and $_{HEa}$miRNA overexpression or 8D) control and $_{HEa}$miRNA hairpin inhibitor transfection with or without concomitant 320 mg/dL ethanol exposure. Bounds of box demarcate limits of 1st and 3rd quartile, line in middle is the median, and whiskers represent the range of data. Representative flow cytometry experiment images are shown on the right in BeWO cytotrophoblasts.

N=10 samples per group, *p<0.05, **p<0.01, ***p<0.001, and ****p<0.0001 by Tukey's HSD.

Figure 9

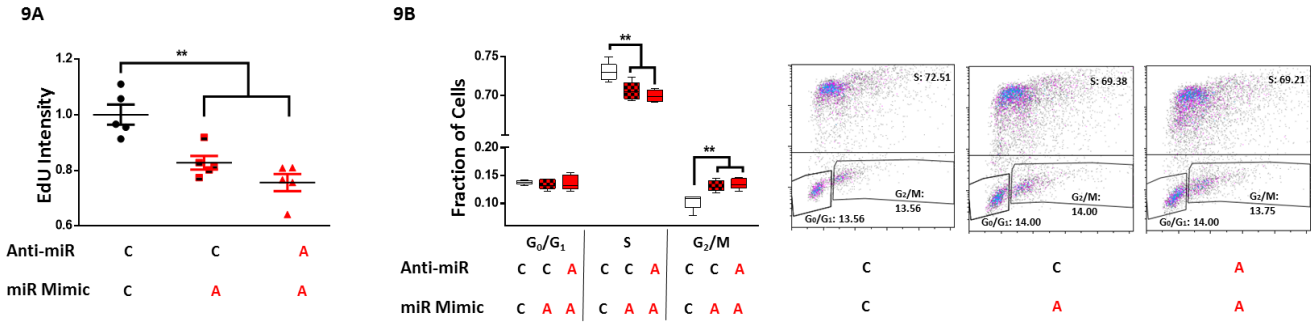

Figure 9: Antagomirs prevent $_{HEa}$miRNA induced cell cycle retardation

9A) Degree of EdU incorporation following control or $_{HEa}$miRNA hairpin inhibitor transfection followed by control or $_{HEa}$miRNA overexpression in BeWO cytotrophoblasts.

9B) Box and whisker plot for the proportion of cells in G_0/G_1, S, or G_2/M phase of the cell cycle following control or $_{HEa}$miRNA hairpin inhibitor transfection followed by control or $_{HEa}$miRNA overexpression in BeWO cytotrophoblasts. Bounds of box demarcate limits of 1st and 3rd quartile, line in middle is the median, and whiskers represent the range of data. Representative flow cytometry experiment images are shown on the right in BeWO cytotrophoblasts.

In subheadings: **C** denotes control miRNA mimic or hairpin whereas **T** denotes $_{HEa}$miRNA mimic or hairpin inhibitor. N=5 samples per group, **p<0.01 by Tukey's HSD.

Figure 10

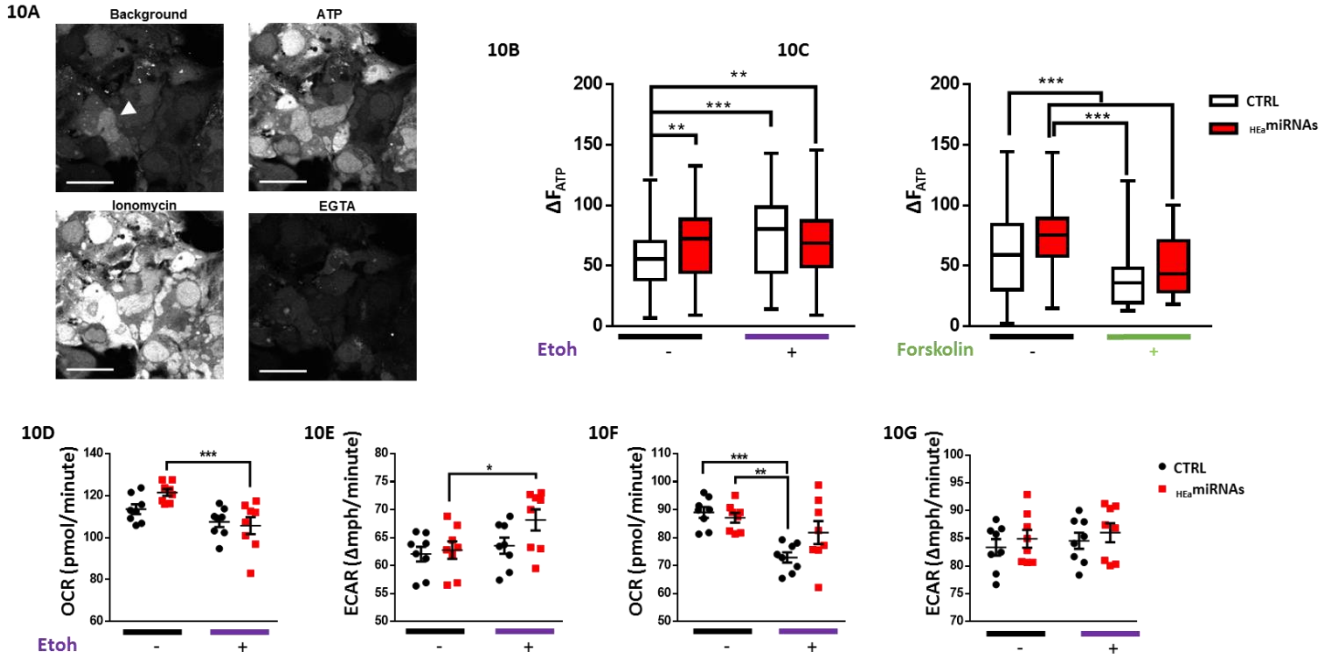

873

874 **Figure 10: $_{HEa}$miRNAs modulate differentiation-associated Ca^{2+} dynamics but have minimal**
875 **effect on the cellular energetics profile**

876 10A) Time-lapse confocal images of BeWO cytotrophoblasts loaded with fluo-4 Ca^{2+} indicator
877 dye under indicated treatment conditions. Arrowhead indicates a fused, multinuclear cell, scale
878 bar is 50µm.
879 10B) Box and whisker plot of intracellular calcium levels following acute ATP administration in
880 BeWO cytotrophoblasts with control and $_{HEa}$miRNA overexpression with or without concomitant
881 320 mg/dL ethanol exposure. Bounds of box demarcate limits of 1st and 3rd quartile, line in
882 middle is the median, and whiskers represent the range of data.
883 10C) Intracellular calcium levels following acute ATP administration in BeWO cytotrophoblasts
884 with control and $_{HEa}$miRNA overexpression with or without 20 µm forskolin treatment.
885 10D) Baseline oxygen consumption rate (OCR), 10E) baseline extracellular acidification rate
886 (ECAR), 10F) stressed OCR, and 10G) stressed ECAR in BeWO cytotrophoblasts with control and
887 $_{HEa}$miRNA overexpression with or without concomitant 320mg/dL ethanol exposure.
888 N=10 samples per group, *p<0.05, **p<0.01, ***p<0.001, and ***p<0.0001 by Tukey's HSD.

Figure 11

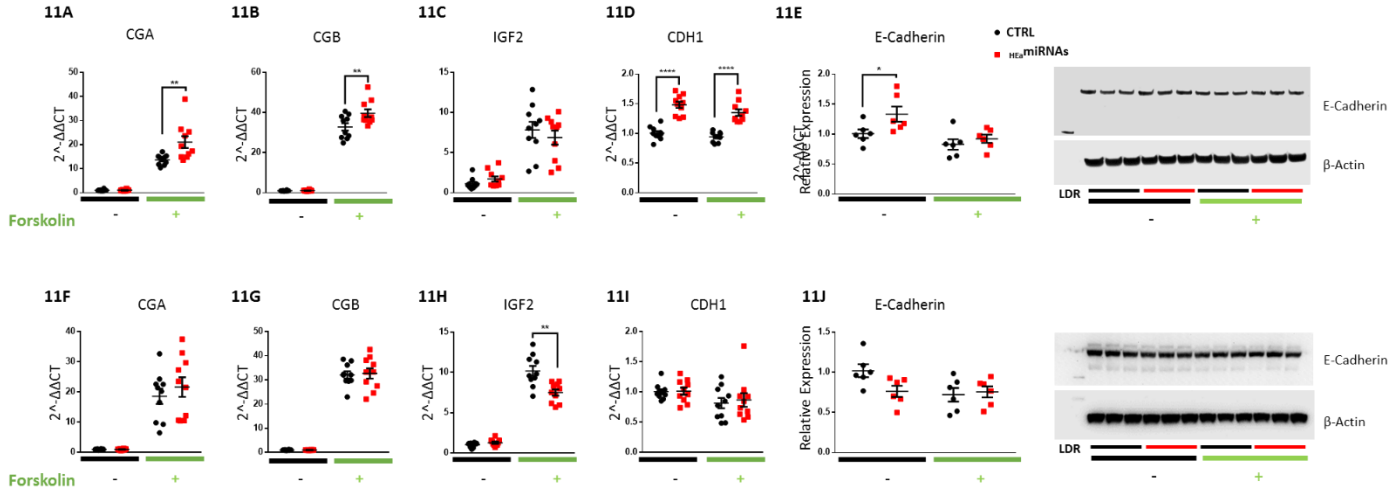

Figure 11: $_{HEa}$miRNAs promote syncytialization dependent hCG production
Expression of 11A) *CGA,* 11B) *CGB,* 11C) *IGF2,* and 11D) *CDH1* transcripts 11E) and densitometric quantification of E-Cadherin protein levels in BeWO cytotrophoblasts following $_{HEa}$miRNAs or control miRNA overexpression with or without 20 µm forskolin treatment. Expression of 11F) *CGA,* 11G) *CGB,* 11H) *IGF2,* and 11I) *CDH1* transcripts 11J) and densitometric quantification of E-Cadherin protein levels in BeWO cytotrophoblasts following $_{HEa}$miRNAs or control hairpin inhibitor transfection with or without 20 µm forskolin treatment. LDR=Molecular Weight Ladder, N=10 samples per group, **p<0.01 and ***p<0.0001 by Tukey's HSD

Figure 12

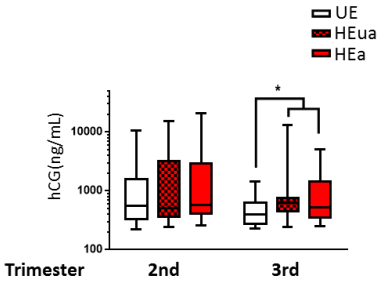

Figure 12: PAE elevates 3rd trimester maternal hCG

Box and whisker plot of 2nd and 3rd trimester maternal hCG levels in UE, HEua, and HEa group mothers of our Ukrainian birth cohort. Bounds of box demarcate limits of 1st and 3rd quartile, line in middle is the median, and whiskers represent the range of data. N=22-23 samples per group, *p=0.03 (Mood's Median Test, χ^2=7.043, df=2).

Figure 13

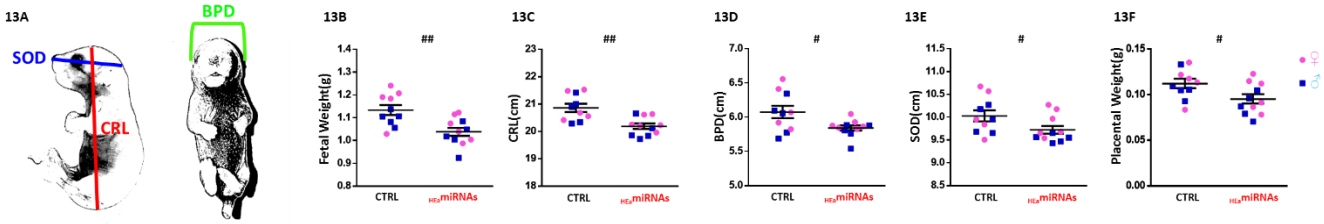

Figure 13: $_{HEa}$miRNAs restrict fetal growth

13A) Schematic for measures of crown rump length (CRL), biparietal diameter (BPD), and snout-occipital distance (SOD).

13B) Fetal weight, 13C) crown-rump length, 13D) biparietal diameter, 13E) snout-occipital distance, 13F) and placental weight at GD18 following administration of control (Ctrl) and $_{HEa}$miRNA mimics to pregnant C57/Bl6 dams on GD10. Dots represent averaged measures of fetal size and placental weights from male and female offspring in independent litters. There were no significant differences in litter sizes [Ctrl: 8.2 and $_{HEa}$miRNAs: 8.5] or sex ratios [Ctrl: 0.86 and $_{HEa}$miRNAs: 1.21] between treatment conditions ($p>0.5$ for all measures). N=5-6 separate litters per treatment condition, $^{\#}p<0.05$, $^{\#\#}p<0.01$ main effect by $_{HEa}$miRNA administration

920 **References**

921 1. ACOG. Committee opinion no. 496: At-risk drinking and alcohol dependence: obstetric and
922 gynecologic implications. *Obstetrics and gynecology.* 2011;118(2 Pt 1):383-8.
923 2. Popova S, Lange S, Probst C, Gmel G, and Rehm J. Estimation of national, regional, and global
924 prevalence of alcohol use during pregnancy and fetal alcohol syndrome: a systematic review and
925 meta-analysis. *The Lancet Global Health.* 2017;5(3):e290-e9.
926 3. SAMHSA. The NSDUH Report: 18 percent of pregnant women drink alcohol during early
927 pregnancy. *NSDUH Report.* 2013.
928 4. Bakhireva LN, Sharkis J, Shrestha S, Miranda-Sohrabji TJ, Williams S, and Miranda RC. Prevalence
929 of Prenatal Alcohol Exposure in the State of Texas as Assessed by Phosphatidylethanol in
930 Newborn Dried Blood Spot Specimens. *Alcohol Clin Exp Res.* 2017;41(5):1004-11.
931 5. Riley EP, Infante MA, and Warren KR. Fetal alcohol spectrum disorders: an overview.
932 *Neuropsychol Rev.* 2011;21(2):73-80.
933 6. May PA, Gossage JP, Kalberg WO, Robinson LK, Buckley D, Manning M, et al. Prevalence and
934 epidemiologic characteristics of FASD from various research methods with an emphasis on
935 recent in-school studies. *Developmental disabilities research reviews.* 2009;15(3):176-92.
936 7. May PA, Blankenship J, Marais AS, Gossage JP, Kalberg WO, Barnard R, et al. Approaching the
937 prevalence of the full spectrum of fetal alcohol spectrum disorders in a South African
938 population-based study. *Alcohol Clin Exp Res.* 2013;37(5):818-30.
939 8. Popova S, Lange S, Probst C, Gmel G, and Rehm J. Estimation of national, regional, and global
940 prevalence of alcohol use during pregnancy and fetal alcohol syndrome: a systematic review and
941 meta-analysis. *Lancet Glob Health.* 2017;5(3):e290-e9.
942 9. Roozen S, Peters GJ, Kok G, Townend D, Nijhuis J, and Curfs L. Worldwide Prevalence of Fetal
943 Alcohol Spectrum Disorders: A Systematic Literature Review Including Meta-Analysis. *Alcohol*
944 *Clin Exp Res.* 2016;40(1):18-32.
945 10. Popova S, Lange S, Burd L, and Rehm J. The Economic Burden of Fetal Alcohol Spectrum Disorder
946 in Canada in 2013. *Alcohol and Alcoholism.* 2016;51(3):367-75.
947 11. Balaraman S, Schafer JJ, Tseng AM, Wertelecki W, Yevtushok L, Zymak-Zakutnya N, et al. Plasma
948 miRNA Profiles in Pregnant Women Predict Infant Outcomes following Prenatal Alcohol
949 Exposure. *PLoS One.* 2016;11(11):e0165081.
950 12. Rossant J, and Cross JC. Placental development: Lessons from mouse mutants. *Nature Reviews*
951 *Genetics.* 2001;2:538.
952 13. E. Davies J, Pollheimer J, Yong HEJ, Kokkinos MI, Kalionis B, Knöfler M, et al. Epithelial-
953 mesenchymal transition during extravillous trophoblast differentiation. *Cell Adhesion &*
954 *Migration.* 2016;10(3):310-21.
955 14. Zhou Y, Damsky CH, and Fisher SJ. Preeclampsia is associated with failure of human
956 cytotrophoblasts to mimic a vascular adhesion phenotype. One cause of defective endovascular
957 invasion in this syndrome? *The Journal of Clinical Investigation.* 1997;99(9):2152-64.
958 15. Damsky CH, and Fisher SJ. Trophoblast pseudo-vasculogenesis: faking it with endothelial
959 adhesion receptors. *Current opinion in cell biology.* 1998;10(5):660-6.
960 16. Brown LM, Lacey HA, Baker PN, and Crocker IP. E-cadherin in the assessment of aberrant
961 placental cytotrophoblast turnover in pregnancies complicated by pre-eclampsia. *Histochemistry*
962 *and cell biology.* 2005;124(6):499-506.
963 17. Fedorova L, Gatto-Weis C, Smaili S, Khurshid N, Shapiro JI, Malhotra D, et al. Down-regulation of
964 the transcription factor snail in the placentas of patients with preeclampsia and in a rat model of
965 preeclampsia. *Reprod Biol Endocrinol.* 2012;10:15.

18. Blechschmidt K, Mylonas I, Mayr D, Schiessl B, Schulze S, Becker KF, et al. Expression of E-cadherin and its repressor snail in placental tissue of normal, preeclamptic and HELLP pregnancies. *Virchows Archiv : an international journal of pathology.* 2007;450(2):195-202.
19. Du L, Kuang L, He F, Tang W, Sun W, and Chen D. Mesenchymal-to-epithelial transition in the placental tissues of patients with preeclampsia. *Hypertension research : official journal of the Japanese Society of Hypertension.* 2017;40(1):67-72.
20. Gundogan F GJ, Ooi JH, Sung J, Qi W, et al. Dual Mechanisms of Ethanol-Impaired Placentation: Experimental Model. *J Clin Exp Pathol.* 2013:3:142. doi: 10.4172/2161-0681.1000142.
21. Tai M, Piskorski A, Kao JCW, Hess LA, M. de la Monte S, and Gündoğan F. Placental Morphology in Fetal Alcohol Spectrum Disorders. *Alcohol and Alcoholism.* 2017;52(2):138-44.
22. Gundogan F, Gilligan J, Qi W, Chen E, Naram R, and de la Monte SM. DOSE EFFECT OF GESTATIONAL ETHANOL EXPOSURE ON PLACENTATION AND FETAL GROWTH. *Placenta.* 2015;36(5):523-30.
23. Gardebjer EM, Cuffe JS, Pantaleon M, Wlodek ME, and Moritz KM. Periconceptional alcohol consumption causes fetal growth restriction and increases glycogen accumulation in the late gestation rat placenta. *Placenta.* 2014;35(1):50-7.
24. Kalisch-Smith JI, Outhwaite JE, Simmons DG, Pantaleon M, and Moritz KM. Alcohol exposure impairs trophoblast survival and alters subtype-specific gene expression in vitro. *Placenta.* 2016;46:87-91.
25. Bahado-Singh RO, Oz AU, Kingston JM, Shahabi S, Hsu CD, and Cole L. The role of hyperglycosylated hCG in trophoblast invasion and the prediction of subsequent pre-eclampsia. *Prenatal diagnosis.* 2002;22(6):478-81.
26. Muller F, Savey L, Le Fiblec B, Bussieres L, Ndayizamba G, Colau JC, et al. Maternal serum human chorionic gonadotropin level at fifteen weeks is a predictor for preeclampsia. *Am J Obstet Gynecol.* 1996;175(1):37-40.
27. Spencer K, Macri JN, Aitken DA, and Connor JM. Free beta-hCG as first-trimester marker for fetal trisomy. *Lancet (London, England).* 1992;339(8807):1480.
28. Spencer K. Evaluation of an assay of the free beta-subunit of choriogonadotropin and its potential value in screening for Down's syndrome. *Clin Chem.* 1991;37(6):809-14.
29. Brady ML, Allan AM, and Caldwell KK. A Limited Access Mouse Model of Prenatal Alcohol Exposure that Produces Long-Lasting Deficits in Hippocampal-Dependent Learning and Memory. *Alcoholism, clinical and experimental research.* 2012;36(3):457-66.
30. Kajimoto K, Allan A, and Cunningham LA. Fate Analysis of Adult Hippocampal Progenitors in a Murine Model of Fetal Alcohol Spectrum Disorder (FASD). *PLoS ONE.* 2013;8(9):e73788.
31. Watson ED, and Cross JC. Development of structures and transport functions in the mouse placenta. *Physiology (Bethesda).* 2005;20:180-93.
32. Gårdebjer EM, Anderson ST, Pantaleon M, Wlodek ME, and Moritz KM. Maternal alcohol intake around the time of conception causes glucose intolerance and insulin insensitivity in rat offspring, which is exacerbated by a postnatal high-fat diet. *The FASEB Journal.* 2015;29(7):2690-701.
33. Lo JO, Schabel MC, Roberts VH, Wang X, Lewandowski KS, Grant KA, et al. First trimester alcohol exposure alters placental perfusion and fetal oxygen availability affecting fetal growth and development in a non-human primate model. *Am J Obstet Gynecol.* 2017;216(3):302.e1-.e8.
34. Grant KA, Leng X, Green HL, Szeliga KT, Rogers LS, and Gonzales SW. Drinking typography established by scheduled induction predicts chronic heavy drinking in a monkey model of ethanol self-administration. *Alcohol Clin Exp Res.* 2008;32(10):1824-38.
35. Carter AM. Animal models of human placentation--a review. *Placenta.* 2007;28 Suppl A:S41-7.

1013 36. Orendi K, Gauster M, Moser G, Meiri H, and Huppertz B. The choriocarcinoma cell line BeWo:
1014 syncytial fusion and expression of syncytium-specific proteins. *Reproduction (Cambridge,*
1015 *England).* 2010;140(5):759-66.
1016 37. Oh SY, Hwang JR, Lee Y, Choi SJ, Kim JS, Kim JH, et al. Isolation of basal membrane proteins from
1017 BeWo cells and their expression in placentas from fetal growth-restricted pregnancies. *Placenta.*
1018 2016;39:24-32.
1019 38. Schindelin J, Arganda-Carreras I, Frise E, Kaynig V, Longair M, Pietzsch T, et al. Fiji: an open-
1020 source platform for biological-image analysis. *Nature methods.* 2012;9(7):676-82.
1021 39. Gong J, Wu Y, Zhang X, Liao Y, Sibanda VL, Liu W, et al. Comprehensive analysis of human small
1022 RNA sequencing data provides insights into expression profiles and miRNA editing. *RNA biology.*
1023 2014;11(11):1375-85.
1024 40. Panwar B, Omenn GS, and Guan Y. miRmine: a database of human miRNA expression profiles.
1025 *Bioinformatics.* 2017;33(10):1554-60.
1026 41. Tsamou M, Vrijens K, Madhloum N, Lefebvre W, Vanpoucke C, and Nawrot TS. Air pollution-
1027 induced placental epigenetic alterations in early life: a candidate miRNA approach. *Epigenetics.*
1028 2018;13(2):135-46.
1029 42. Shi Z, Zhao C, Guo X, Ding H, Cui Y, Shen R, et al. Differential expression of microRNAs in omental
1030 adipose tissue from gestational diabetes mellitus subjects reveals miR-222 as a regulator of
1031 ERalpha expression in estrogen-induced insulin resistance. *Endocrinology.* 2014;155(5):1982-90.
1032 43. McAdams RM, McPherson RJ, Beyer RP, Bammler TK, Farin FM, and Juul SE. Dose-dependent
1033 effects of morphine exposure on mRNA and microRNA (miR) expression in hippocampus of
1034 stressed neonatal mice. *PLoS One.* 2015;10(4):e0123047.
1035 44. Ignacio C, Mooney SM, and Middleton FA. Effects of Acute Prenatal Exposure to Ethanol on
1036 microRNA Expression are Ameliorated by Social Enrichment. *Frontiers in pediatrics.* 2014;2:103.
1037 45. Liu XD, Wu X, Yin YL, Liu YQ, Geng MM, Yang HS, et al. Effects of dietary L-arginine or N-
1038 carbamylglutamate supplementation during late gestation of sows on the miR-15b/16, miR-
1039 221/222, VEGFA and eNOS expression in umbilical vein. *Amino acids.* 2012;42(6):2111-9.
1040 46. Nemoto T, Kakinuma Y, and Shibasaki T. Impaired miR449a-induced downregulation of Crhr1
1041 expression in low-birth-weight rats. *The Journal of endocrinology.* 2015;224(2):195-203.
1042 47. Nardelli C, Granata I, Iaffaldano L, D'Argenio V, Del Monaco V, Maruotti GM, et al. miR-138/miR-
1043 222 Overexpression Characterizes the miRNome of Amniotic Mesenchymal Stem Cells in
1044 Obesity. *Stem cells and development.* 2017;26(1):4-14.
1045 48. Baker BC, Mackie FL, Lean SC, Greenwood SL, Heazell AEP, Forbes K, et al. Placental dysfunction
1046 is associated with altered microRNA expression in pregnant women with low folate status.
1047 *Molecular nutrition & food research.* 2017;61(8).
1048 49. Salihu HM, Kornosky JL, Lynch O, Alio AP, August EM, and Marty PJ. Impact of prenatal alcohol
1049 consumption on placenta-associated syndromes. *Alcohol.* 2011;45(1):73-9.
1050 50. Khong TY. Placental vascular development and neonatal outcome. *Seminars in neonatology : SN.*
1051 2004;9(4):255-63.
1052 51. Ray JG, Vermeulen MJ, Schull MJ, and Redelmeier DA. Cardiovascular health after maternal
1053 placental syndromes (CHAMPS): population-based retrospective cohort study. *Lancet (London,*
1054 *England).* 2005;366(9499):1797-803.
1055 52. Wang D, Na Q, Song WW, and Song GY. Altered Expression of miR-518b and miR-519a in the
1056 placenta is associated with low fetal birth weight. *American journal of perinatology.*
1057 2014;31(9):729-34.
1058 53. Wang JM, Gu Y, Zhang Y, Yang Q, Zhang X, Yin L, et al. Deep-sequencing identification of
1059 differentially expressed miRNAs in decidua and villus of recurrent miscarriage patients. *Archives*
1060 *of gynecology and obstetrics.* 2016;293(5):1125-35.

1061 54. Hromadnikova I, Kotlabova K, Ondrackova M, Pirkova P, Kestlerova A, Novotna V, et al.
1062 Expression profile of C19MC microRNAs in placental tissue in pregnancy-related complications.
1063 *DNA and cell biology.* 2015;34(6):437-57.
1064 55. Hromadnikova I, Kotlabova K, Ivankova K, and Krofta L. Expression profile of C19MC microRNAs
1065 in placental tissue of patients with preterm prelabor rupture of membranes and spontaneous
1066 preterm birth. *Molecular medicine reports.* 2017;16(4):3849-62.
1067 56. Timofeeva AV, Gusar VA, Kan NE, Prozorovskaya KN, Karapetyan AO, Bayev OR, et al.
1068 Identification of potential early biomarkers of preeclampsia. *Placenta.* 2018;61:61-71.
1069 57. Dong F, Zhang Y, Xia F, Yang Y, Xiong S, Jin L, et al. Genome-wide miRNA profiling of villus and
1070 decidua of recurrent spontaneous abortion patients. *Reproduction (Cambridge, England).*
1071 2014;148(1):33-41.
1072 58. Hu Y, Li P, Hao S, Liu L, Zhao J, and Hou Y. Differential expression of microRNAs in the placentae
1073 of Chinese patients with severe pre-eclampsia. *Clinical chemistry and laboratory medicine.*
1074 2009;47(8):923-9.
1075 59. Murphy MS, Casselman RC, Tayade C, and Smith GN. Differential expression of plasma
1076 microRNA in preeclamptic patients at delivery and 1 year postpartum. *Am J Obstet Gynecol.*
1077 2015;213(3):367.e1-9.
1078 60. Bidarimath M, Edwards AK, Wessels JM, Khalaj K, Kridli RT, and Tayade C. Distinct microRNA
1079 expression in endometrial lymphocytes, endometrium, and trophoblast during spontaneous
1080 porcine fetal loss. *Journal of reproductive immunology.* 2015;107:64-79.
1081 61. Gao Y, She R, Wang Q, Li Y, and Zhang H. Up-regulation of miR-299 suppressed the invasion and
1082 migration of HTR-8/SVneo trophoblast cells partly via targeting HDAC2 in pre-eclampsia.
1083 *Biomedicine & pharmacotherapy = Biomedecine & pharmacotherapie.* 2018;97:1222-8.
1084 62. Sandrim VC, Luizon MR, Palei AC, Tanus-Santos JE, and Cavalli RC. Circulating microRNA
1085 expression profiles in pre-eclampsia: evidence of increased miR-885-5p levels. *BJOG : an*
1086 *international journal of obstetrics and gynaecology.* 2016;123(13):2120-8.
1087 63. Rodosthenous RS, Burris HH, Sanders AP, Just AC, Dereix AE, Svensson K, et al. Second trimester
1088 extracellular microRNAs in maternal blood and fetal growth: An exploratory study. *Epigenetics.*
1089 2017;12(9):804-10.
1090 64. Martinez-Fierro ML, Garza-Veloz I, Gutierrez-Arteaga C, Delgado-Enciso I, Barbosa-Cisneros OY,
1091 Flores-Morales V, et al. Circulating levels of specific members of chromosome 19 microRNA
1092 cluster are associated with preeclampsia development. *Archives of gynecology and obstetrics.*
1093 2018;297(2):365-71.
1094 65. Yang S, Li H, Ge Q, Guo L, and Chen F. Deregulated microRNA species in the plasma and placenta
1095 of patients with preeclampsia. *Molecular medicine reports.* 2015;12(1):527-34.
1096 66. Hromadnikova I, Kotlabova K, Ivankova K, and Krofta L. First trimester screening of circulating
1097 C19MC microRNAs and the evaluation of their potential to predict the onset of preeclampsia
1098 and IUGR. *PLOS ONE.* 2017;12(2):e0171756.
1099 67. Zhang M, Muralimanoharan S, Wortman AC, and Mendelson CR. Primate-specific miR-515 family
1100 members inhibit key genes in human trophoblast differentiation and are upregulated in
1101 preeclampsia. *Proceedings of the National Academy of Sciences of the United States of America.*
1102 2016;113(45):E7069-E76.
1103 68. Mei Z, Huang B, Mo Y, and Fan J. An exploratory study into the role of miR-204-5p in pregnancy-
1104 induced hypertension. *Experimental and therapeutic medicine.* 2017;13(5):1711-8.
1105 69. Choi SY, Yun J, Lee OJ, Han HS, Yeo MK, Lee MA, et al. MicroRNA expression profiles in placenta
1106 with severe preeclampsia using a PNA-based microarray. *Placenta.* 2013;34(9):799-804.
1107 70. Kaufmann P, Black S, and Huppertz B. Endovascular trophoblast invasion: implications for the
1108 pathogenesis of intrauterine growth retardation and preeclampsia. *Biol Reprod.* 2003;69(1):1-7.

1109 71. Barrientos G, Pussetto M, Rose M, Staff AC, Blois SM, and Toblli JE. Defective trophoblast
1110 invasion underlies fetal growth restriction and preeclampsia-like symptoms in the stroke-prone
1111 spontaneously hypertensive rat. *Molecular human reproduction.* 2017;23(7):509-19.
1112 72. Roberts JM, and Escudero C. The placenta in preeclampsia. *Pregnancy hypertension.*
1113 2012;2(2):72-83.
1114 73. Fisher SJ. Why is placentation abnormal in preeclampsia? *American journal of obstetrics and*
1115 *gynecology.* 2015;213(4 0):S115-S22.
1116 74. Crosley EJ, Elliot MG, Christians JK, and Crespi BJ. Placental invasion, preeclampsia risk and
1117 adaptive molecular evolution at the origin of the great apes: evidence from genome-wide
1118 analyses. *Placenta.* 2013;34(2):127-32.
1119 75. Lyall F, Bulmer JN, Duffie E, Cousins F, Theriault A, and Robson SC. Human Trophoblast Invasion
1120 and Spiral Artery Transformation : The Role of PECAM-1 in Normal Pregnancy, Preeclampsia, and
1121 Fetal Growth Restriction. *The American Journal of Pathology.* 2001;158(5):1713-21.
1122 76. Goldman-Wohl D, and Yagel S. Regulation of trophoblast invasion: from normal implantation to
1123 pre-eclampsia. *Molecular and cellular endocrinology.* 2002;187(1-2):233-8.
1124 77. Balaraman S, Lunde ER, Sawant O, Cudd TA, Washburn SE, and Miranda RC. Maternal and
1125 neonatal plasma microRNA biomarkers for fetal alcohol exposure in an ovine model. *Alcohol Clin*
1126 *Exp Res.* 2014;38(5):1390-400.
1127 78. Vicovac L, and Aplin JD. Epithelial-mesenchymal transition during trophoblast differentiation.
1128 *Acta anatomica.* 1996;156(3):202-16.
1129 79. Knöfler M, and Pollheimer J. Human placental trophoblast invasion and differentiation: a
1130 particular focus on Wnt signaling. *Frontiers in Genetics.* 2013;4:190.
1131 80. Barrak J, Msheik H, Abou-Kheir W, and Daoud G. Assessment of different trophoblast cell lines
1132 as in vitro models for placental development. *Placenta.* 2016;45:106.
1133 81. Lovisa S, LeBleu VS, Tampe B, Sugimoto H, Vadnagara K, Carstens JL, et al. Epithelial-to-
1134 mesenchymal transition induces cell cycle arrest and parenchymal damage in renal fibrosis.
1135 *Nature medicine.* 2015;21(9):998-1009.
1136 82. Vega S, Morales AV, Ocana OH, Valdes F, Fabregat I, and Nieto MA. Snail blocks the cell cycle
1137 and confers resistance to cell death. *Genes & development.* 2004;18(10):1131-43.
1138 83. Moreau R, Hamel A, Daoud G, Simoneau L, and Lafond J. Expression of calcium channels along
1139 the differentiation of cultured trophoblast cells from human term placenta. *Biol Reprod.*
1140 2002;67(5):1473-9.
1141 84. Jones CJ, and Fox H. Ultrastructure of the normal human placenta. *Electron microscopy reviews.*
1142 1991;4(1):129-78.
1143 85. Spaans F, Melgert BN, Chiang C, Borghuis T, Klok PA, de Vos P, et al. Extracellular ATP decreases
1144 trophoblast invasion, spiral artery remodeling and immune cells in the mesometrial triangle in
1145 pregnant rats. *Placenta.* 2014;35(8):587-95.
1146 86. Karl PI, Chusid J, Tagoe C, and Fisher SE. Ca2+ flux in human placental trophoblasts. *Am J Physiol.*
1147 1997;272(6 Pt 1):C1776-80.
1148 87. Roberts VH, Waters LH, and Powell T. Purinergic receptor expression and activation in first
1149 trimester and term human placenta. *Placenta.* 2007;28(4):339-47.
1150 88. Halmesmaki E, Autti I, Granstrom ML, Stenman UH, and Ylikorkala O. Estradiol, estriol,
1151 progesterone, prolactin, and human chorionic gonadotropin in pregnant women with alcohol
1152 abuse. *J Clin Endocrinol Metab.* 1987;64(1):153-6.
1153 89. . *Encyclopedia of Statistical Sciences*.
1154 90. Edelstam G, Karlsson C, Westgren M, Lowbeer C, and Swahn ML. Human chorionic gonadatropin
1155 (hCG) during third trimester pregnancy. *Scandinavian journal of clinical and laboratory*
1156 *investigation.* 2007;67(5):519-25.

1157 91. Soares MJ, Chakraborty D, Rumi MAK, Konno T, and Renaud SJ. Rat Placentation: An
1158 Experimental Model For Investigating The Hemochorial Maternal-Fetal Interface. *Placenta.*
1159 2012;33(4):233-43.
1160 92. Grigsby PL. Animal Models to Study Placental Development and Function throughout Normal
1161 and Dysfunctional Human Pregnancy. *Seminars in reproductive medicine.* 2016;34(1):11-6.
1162 93. Vercruysse L, Caluwaerts S, Luyten C, and Pijnenborg R. Interstitial trophoblast invasion in the
1163 decidua and mesometrial triangle during the last third of pregnancy in the rat. *Placenta.*
1164 2006;27(1):22-33.
1165 94. Silva JF, and Serakides R. Intrauterine trophoblast migration: A comparative view of humans and
1166 rodents. *Cell Adhesion & Migration.* 2016;10(1-2):88-110.
1167 95. Adamson SL, Lu Y, Whiteley KJ, Holmyard D, Hemberger M, Pfarrer C, et al. Interactions between
1168 Trophoblast Cells and the Maternal and Fetal Circulation in the Mouse Placenta. *Developmental*
1169 *Biology.* 2002;250(2):358-73.
1170 96. Kurtzman JT, Wilson H, and Rao CV. A Proposed Role for hCG in Clinical Obstetrics. *Semin Reprod*
1171 *Med.* 2001;19(01):063-8.
1172 97. Furcron A-E, Romero R, Mial TN, Balancio A, Panaitescu B, Hassan SS, et al. Human Chorionic
1173 Gonadotropin Has Anti-Inflammatory Effects at the Maternal-Fetal Interface and Prevents
1174 Endotoxin-Induced Preterm Birth, but Causes Dystocia and Fetal Compromise in Mice. *Biology of*
1175 *Reproduction.* 2016;94(6):136.
1176 98. Henderson GI, Hoyumpa AM, Jr., McClain C, and Schenker S. The effects of chronic and acute
1177 alcohol administration on fetal development in the rat. *Alcohol Clin Exp Res.* 1979;3(2):99-106.
1178 99. O'Leary-Moore SK, Parnell SE, Godin EA, Dehart DB, Ament JJ, Khan AA, et al. Magnetic
1179 resonance microscopy-based analyses of the brains of normal and ethanol-exposed fetal mice.
1180 *Birth Defects Res A Clin Mol Teratol.* 2010;88(11):953-64.
1181 100. Bake S, Tingling JD, and Miranda RC. Ethanol exposure during pregnancy persistently attenuates
1182 cranially directed blood flow in the developing fetus: evidence from ultrasound imaging in a
1183 murine second trimester equivalent model. *Alcohol Clin Exp Res.* 2012;36(5):748-58.
1184 101. Gaccioli F, and Lager S. Placental Nutrient Transport and Intrauterine Growth Restriction.
1185 *Frontiers in Physiology.* 2016;7:40.
1186 102. Haggarty P, Abramovich DR, and Page K. The effect of maternal smoking and ethanol on fatty
1187 acid transport by the human placenta. *The British journal of nutrition.* 2002;87(3):247-52.
1188 103. Lui S, Jones RL, Robinson NJ, Greenwood SL, Aplin JD, and Tower CL. Detrimental Effects of
1189 Ethanol and Its Metabolite Acetaldehyde, on First Trimester Human Placental Cell Turnover and
1190 Function. *PLOS ONE.* 2014;9(2):e87328.
1191 104. Rufer ES, Tran TD, Attridge MM, Andrzejewski ME, Flentke GR, and Smith SM. Adequacy of
1192 Maternal Iron Status Protects against Behavioral, Neuroanatomical, and Growth Deficits in Fetal
1193 Alcohol Spectrum Disorders. *PLoS ONE.* 2012;7(10):e47499.
1194 105. Huebner SM, Blohowiak SE, Kling PJ, and Smith SM. Prenatal Alcohol Exposure Alters Fetal Iron
1195 Distribution and Elevates Hepatic Hepcidin in a Rat Model of Fetal Alcohol Spectrum Disorders.
1196 *The Journal of Nutrition.* 2016;146(6):1180-8.
1197 106. Xie L, Mouillet J-F, Chu T, Parks WT, Sadovsky E, Knöfler M, et al. C19MC MicroRNAs Regulate
1198 the Migration of Human Trophoblasts. *Endocrinology.* 2014;155(12):4975-85.
1199 107. Salomon C, Torres MJ, Kobayashi M, Scholz-Romero K, Sobrevia L, Dobierzewska A, et al. A
1200 Gestational Profile of Placental Exosomes in Maternal Plasma and Their Effects on Endothelial
1201 Cell Migration. *PLOS ONE.* 2014;9(6):e98667.
1202 108. Ouyang Y, Mouillet J-F, Coyne CB, and Sadovsky Y. Placenta-specific microRNAs in exosomes –
1203 good things come in nano-packages. *Placenta.* 2014;35 Suppl:S69-S73.

1204 109. Sabapatha A, Gercel-Taylor C, and Taylor DD. Specific isolation of placenta-derived exosomes
1205 from the circulation of pregnant women and their immunoregulatory consequences. *American*
1206 *journal of reproductive immunology (New York, NY : 1989).* 2006;56(5-6):345-55.
1207 110. Nair S, and Salomon C. Extracellular vesicles and their immunomodulatory functions in
1208 pregnancy. *Seminars in immunopathology.* 2018.
1209 111. Delorme-Axford E, Donker RB, Mouillet J-F, Chu T, Bayer A, Ouyang Y, et al. Human placental
1210 trophoblasts confer viral resistance to recipient cells. *Proceedings of the National Academy of*
1211 *Sciences of the United States of America.* 2013;110(29):12048-53.
1212 112. Donker RB, Mouillet JF, Chu T, Hubel CA, Stolz DB, Morelli AE, et al. The expression profile of
1213 C19MC microRNAs in primary human trophoblast cells and exosomes. *Molecular human*
1214 *reproduction.* 2012;18(8):417-24.
1215 113. Cronqvist T, Tannetta D, Mörgelin M, Belting M, Sargent I, Familari M, et al. Syncytiotrophoblast
1216 derived extracellular vesicles transfer functional placental miRNAs to primary human endothelial
1217 cells. *Scientific Reports.* 2017;7(1):4558.
1218 114. Smith SM, Garic A, Flentke GR, and Berres ME. Neural Crest Development in Fetal Alcohol
1219 Syndrome. *Birth defects research Part C, Embryo today : reviews.* 2014;102(3):210-20.
1220 115. Kalcheim C. Epithelial–Mesenchymal Transitions during Neural Crest and Somite Development.
1221 *Journal of Clinical Medicine.* 2016;5(1):1.
1222 116. Yang J, Qiu H, Qu P, Zhang R, Zeng L, and Yan H. Prenatal Alcohol Exposure and Congenital Heart
1223 Defects: A Meta-Analysis. *PLoS ONE.* 2015;10(6):e0130681.
1224 117. Burd L, Deal E, Rios R, Adickes E, Wynne J, and Klug MG. Congenital heart defects and fetal
1225 alcohol spectrum disorders. *Congenital heart disease.* 2007;2(4):250-5.
1226 118. Serrano M, Han M, Brinez P, and Linask KK. Fetal alcohol syndrome: cardiac birth defects in mice
1227 and prevention with folate. *Am J Obstet Gynecol.* 2010;203(1):75.e7-.e15.
1228 119. Sarmah S, and Marrs JA. Complex cardiac defects after ethanol exposure during discrete
1229 cardiogenic events in zebrafish: Prevention with folic acid. *Developmental dynamics : an official*
1230 *publication of the American Association of Anatomists.* 2013;242(10):1184-201.
1231 120. Combs MD, and Yutzey KE. Heart Valve Development: Regulatory networks in development and
1232 disease. *Circulation research.* 2009;105(5):408-21.
1233 121. Lin C-J, Lin C-Y, Chen C-H, Zhou B, and Chang C-P. Partitioning the heart: mechanisms of cardiac
1234 septation and valve development. *Development (Cambridge, England).* 2012;139(18):3277-99.
1235 122. Janssen HL, Reesink HW, Lawitz EJ, Zeuzem S, Rodriguez-Torres M, Patel K, et al. Treatment of
1236 HCV infection by targeting microRNA. *The New England journal of medicine.* 2013;368(18):1685-
1237 94.
1238 123. Beg MS, Brenner AJ, Sachdev J, Borad M, Kang YK, Stoudemire J, et al. Phase I study of MRX34, a
1239 liposomal miR-34a mimic, administered twice weekly in patients with advanced solid tumors.
1240 *Invest New Drugs.* 2017;35(2):180-8.
1241 124. Sathyan P, Golden HB, and Miranda RC. Competing interactions between micro-RNAs determine
1242 neural progenitor survival and proliferation after ethanol exposure: evidence from an ex vivo
1243 model of the fetal cerebral cortical neuroepithelium. *J Neurosci.* 2007;27(32):8546-57.
1244 125. Huang W, Tian SS, Hang PZ, Sun C, Guo J, and Du ZM. Combination of microRNA-21 and
1245 microRNA-146a Attenuates Cardiac Dysfunction and Apoptosis During Acute Myocardial
1246 Infarction in Mice. *Molecular therapy Nucleic acids.* 2016;5:e296.

1247